Characterization, Implementation and Control of Paramagnetic Beads for the Extraction of Nucleic Acids from Patient Bio-Fluids in Point of Need Microfluidics Systems

by

Shilpita Biswas

A Thesis Presented in Partial Fulfillment
of the Requirements for the Degree
Master of Science

Approved April 2021 by the
Graduate Supervisory Committee:

Jennifer Blain Christen, Chair
Sule Ozev
Michael Goryll

ARIZONA STATE UNIVERSITY

May 2021

ABSTRACT

Point-of-Care diagnostics is one of the most popular fields of research in bio-medicine today because of its portability, speed of response, convenience and quality assurance. One of the most important steps in such a device is to prepare and purify the sample by extracting the nucleic acids, for which small spherical magnetic particles called magnetic beads are often used in laboratories. Even though magnetic beads have the ability to isolate DNA or RNA from bio-samples in their purified form, integrating these into a microfluidic point-of-need testing kit is still a bit of a challenge. In this thesis, the possibility of integrating paramagnetic beads instead of silica-coated dynabeads, has been evaluated with respect to a point-of-need SARS-CoV-2 virus testing kit. This project is a comparative study between five different sizes of carboxyl-coated paramagnetic beads with reference to silica-coated dynabeads, and how each of them behave in a microcapillary chip in presence of magnetic fields of different strengths. The diameters and velocities of the beads have been calculated using different types of microscopic imaging techniques. The washing and elution steps of an extraction process have been recreated using syringe pump, microcapillary channels and permanent magnets, based on which those parameters of the beads have been studied which are essential for extraction behaviour. The yield efficiency of the beads have also been analysed by using these to extract Salmon DNA. Overall, furthering this research will improve the sensitivity and specificity for any low-cost nucleic-acid based point-of-care testing device.

ACKNOWLEDGMENTS

My journey at Arizona State University as a Master's student has been a wonderful learning experience of two years. As I stand today at the threshold of my graduation, I would first like to thank my advisor and committee chair, Professor Jennifer Blain Christen, for giving me the wonderful opportunity to work in her laboratory and for providing invaluable guidance and motivation through the course of this research. I learnt so much from my collaborative work with the different members of the lab and I am immensely grateful to have been given this opportunity.

I would next like to express my sincere gratitude towards Professor Sule Ozev and Professor Michael Goryll, for willing to serve as members of the defense committee and for providing their insightful suggestions and feedback.

Next, I would like to thank all the members of the lab without whom I would not have managed to defend my thesis and complete my work on time. I would like to thank Vi Nguyen and Siril Arockiam for their invaluable guidance throughout my thesis project, I would also like to thank Bat-El Shabtai, Michael Hansen, Greg Durnan and Clifford Anderson for their constant help, valuable advice, and for offering assistance with the theoretical and practical aspects of this project.

Last but not the least, I am extremely grateful to my family and friends for supporting me unconditionally throughout this journey. But, most of all, I would like to thank my parents, Ashis Kumar Biswas and Sharmila Biswas without whom I would never have dared to dream in the first place. My parents have taught me from a very young age to pursue my dreams relentlessly, come what may. That encouragement gave me the strength to travel so far from my home country and work hard towards my studies and thus, my graduation.

I thank all of you for inspiring me to be a better human being everyday, as I strive to make my mark in the world outside the confines of this university.

TABLE OF CONTENTS

CHAPTER Page

LIST OF TABLES

Table Page

LIST OF FIGURES

Figure Page

Figure Page

Chapter 1

INTRODUCTION

1.1 Motivation

Point-of-Care (PoC) diagnostics is one of the most popular fields of research in present times. The world today demands technology which would fit not only in their pockets but in the palms of one's hands - be it a cell phone or an ear-pod or even a medical diagnostic device. These devices have widespread use nowadays as testing can be done by people who do not need to be trained in clinical laboratory sciences. Even in hospitals nowadays, we see widespread use of these devices because of its portability, the quick feedback or results of the medical tests, convenience, speed of response and quality assurance. All we need is one drop of blood or of any bio-fluid sample from the human body and within a matter of seconds, we have our test results in front of us.

One of the most important steps in a PoC device is to prepare and purify the sample, especially extracting the purified nucleic acids for further molecular-based diagnostics(Byrnes *et al.* (2015)). Now the question is how do we isolate the DNA or RNA strands from the biological samples? This is where the concept of magnetic beads or magnetic micro particles come into consideration. The magnetic beads ranging from a size of a few micrometers to almost 120 micrometers in diameter have the ability to separate different types of cells based on their magnetic properties and also to extract and isolate DNA/RNA from samples in its purified form based on the type of coating around the beads. Magnetic beads used in microfluidic channels have been a revolutionary force in the development of cheap, efficient and cost-effective

handheld PoC devices.

The magnetic beads have a range of applications in both diagnosis and therapy in the bio-medical field. In Magnetic Resonance Imaging (MRI) and Radiotherapy, magnetic nano-particles are used as contrast agents for imaging purposes. Also, from the diagnostic point of view, magnetic beads, nowadays, are being used largely for targeted drug delivery where these particles are bound with drugs and by external application of magnetic field, manipulated into moving through the different pathways of the human body as they deliver the drugs in the deepest parts of the brain or regions of the body, harbouring deadly tumors or cancerous cells. Even in micro-electromechanical systems or MEMS, there is a popular concept of magnetic chaining which is used for mixing fluids effectively in microcapillary channels. When rotating alternating magnetic field is applied, the beads form a chain like structure, thus moving or rotating along with the orientation of the field and resulting in proper mixing of the fluids pipetted into the microfluidics systems (Ruffert (2016)). All these applications along with that of extracting the nucleic acids have made it evident that a proper study of the magnetic bead properties is required in order to design a cost-effective, robust and efficient PoC device with the magnetic beads integrated within the microcapillary channels.

1.2 Objective

The initial objective of this thesis was to design an electromagnetic circuit which would attract the magnetic beads while we use them for attracting the RNA of SARS-CoV-2 virus from the human saliva samples and at the same time, be small enough to be incorporated into a PoC testing kit. Solenoid structures with magnet wires and iron cores were designed whose magnetic strength could be varied by changing the current and voltage applied. Certain challenges were encountered which led to

the analysis of the behaviour of the magnetic beads in presence of different types of permanent magnets of varying magnetic strengths, materials and sizes. In fact, different types of beads were studied too from sizes ranging from as low as 1.17 μm to as high as 120 μm in diameter. Parameters like diameter, velocity, flow rate of the beads were measured and studied using different types of microscopes and imaging techniques, thus giving an insight into the characterization of the magnetic beads in presence of both electromagnets and permanent magnets. Lastly, the beads were even used to extract Salmon DNA to analyse which beads performed the best based on the concentration of DNA extracted with reference to the DNA concentration in original sample.

The goal was to develop an understanding of which type of magnetic bead would be suitable for implementation in a handheld PoC device in terms of size, efficiency and capability to attract the nucleic acids and also in terms of yield efficiency. At the same time, being able to control the magnetic strength of the magnet used to attract the beads, provides the user with a kind of flexibility to control the field strength and how it might be implemented is worth exploring while developing an energy-efficient, cost-effective and robust PoC device.

1.3 Thesis Organization

In Chapter 2, a background study on the para magnetic and superparamagnetic beads is provided along with an in-depth explanation of how those are used in the extraction and isolation of nucleic acids from bio samples. An insight into the RT-PCR method and why the magnetic beads are used in the first place is also provided. This chapter also delves into the different types of magnetic beads used in this study and their parameters. Chapter 3 delves into the different types of permanent magnets and electromagnets and their respective properties. In Chapter 4, an in-depth literature

review is done about the various techniques used till date, in studies all round the world. In this chapter, certain mathematical derivations with regards to different parameters of magnetic beads have been shown too. It also details the various studies conducted on magnetic beads and their characteristics and the motivation behind this project. In Chapter 5, detailed explanation for the experiments conducted along with the methods and materials used to collect data have been discussed. The final results and observations obtained during the course of the experiments are explained in Chapter 6. Finally, Chapter 7 concludes this thesis project report with a summary of the challenges faced in the course of the project and how the detailed study has impacted or contributed to the field of PoC devices. It also discusses future scope of work and further improvements in related topics.

Chapter 2

BACKGROUND ON THE BEADS

2.1 RT-PCR Method in COVID-19 PoC Device

For any PoC device used for detecting the presence of any type of viral infection detecting the presence of any type of viral infection within the human body, the viral DNA is replicated into billions of copies so that proper analysis can be carried out. Often, this is done using standard PCR (Polymerase Chain Reaction) procedures. The SARS-CoV-2 virus on the other hand has a single long stranded RNA genome. Therefore the viral RNA needs to be processed first using the RT-PCR method which stands for Reverse Transcriptase- Polymerase Chain Reaction.

Reverse Transcription is the process of converting an RNA strand to its corresponding DNA, after which the process is similar to a standard PCR. PCR consists of 3 steps- Denaturation, Annealing and Extension.

- Denaturation: It is the process by which the two complementary strands of the DNA are separated out. This denaturation or opening up of the DNA strands is performed at a high temperature of 95 degrees celsius as shown in 2.1.

- Annealing: The second step of PCR known as Annealing is the process of finding the target region of DNA which will be copied or amplified again and again. Short strands of custom-made DNA molecules which are often known as primers help us find these target sequences due to which they are often referred to as genetic bookmarks. Annealing takes place roughly within the temperature range of 50 degrees-65 degrees celsius. Each reaction has two types of primers -

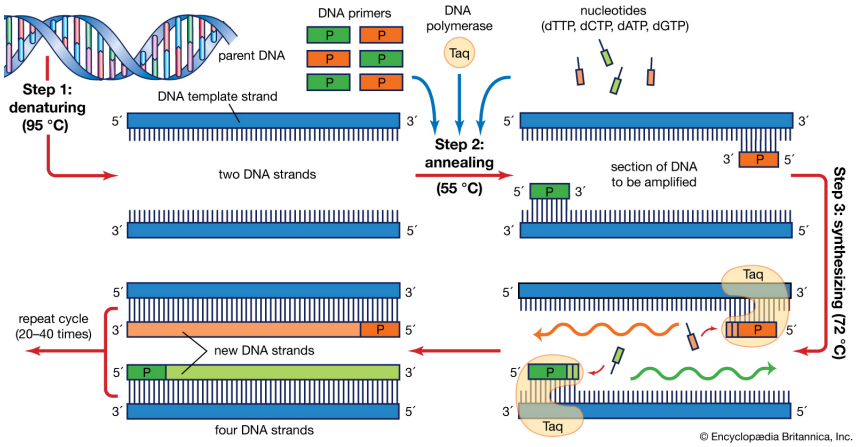

Figure 2.1: Steps of Polymerase Chain Reaction. From Britannica (2019)

forward and reverse. The forward primers will match a sequence on one strand of DNA at the beginning of the region we want to amplify, from 5' to 3' direction; while the reverse primer will match the end of the region at the other strand from 3' to 5' direction. Primers are usually 20 bases long.

When we cool our reaction down, the primers will anneal or stick to their complementary portions of the template DNA strands. By lowering the temperature, we allow the hydrogen bonds to be formed between the template strand and the primers at areas where the sequence is complementary. In order to increase the chances of annealing, we usually add a lot of extra primers so that we can prevent the DNA strands from sticking back with each other and instead stick with the primers inserted. Annealing time may vary from as low as 5 seconds to as long as 30 seconds.

- Extension: The final step is the one called Extension where the annealed part is extended throughout the entire length of DNA to make exact copies of them. For this step, we usually require an enzyme called DNA Polymerase which finds the ends of the short double-stranded regions of the DNA where the primers have bound. It then moves along the DNA base by base in the 5' to 3' direction

and adds the correct complementary DNA nucleotide as it moves. The optimal temperature for the polymerase is 72 degrees celsius and the time of extension usually varies from 10 seconds to a few minutes.

2.2 Extraction and Isolation Process of Beads

As mentioned earlier, one of the critical functions of magnetic beads for molecular diagnostics is their ability to extract and isolate the nucleic acids from the biological sample collected. In the Covid-19 PoC Device, before we perform the RT-PCR our first step should be to isolate the single stranded RNA from the saliva sample collected from the human body. This is where the magnetic beads come into play.

The nucleic acid extraction process usually consists of four stages - lyse, bind, wash and elute as shown in figure 2.2. In the first step, lysis buffer along with Proteinase K and other reagents are added to 100μl of sample which ruptures the cells and release the nucleic acids. In the binding stage, selective binding of nucleic acids occur to a specific carrier based on its chemical composition and under certain conditions, while other impurities such as proteins, lipids, polysaccharides etc. are left behind as the supernatant. In the third step, the supernatant in its liquid phase is washed repeatedly using a wash buffer solution and 80% ethanol so that only the nucleic acids bound to the carrier are left behind. Finally, in the elute step, the elution buffer, usually water, is added which releases the hydrophilic nucleic acids from the carriers and thus, the purified DNA or RNA strands are isolated successfully for further processing.

The traditional method of performing this entire extraction process is by using a spin-column centrifuge. In the binding step, the sample along with a binding solution is placed in a spin column which is subjected to repeated centrifugation. The centrifuge forces the nucleic acids to pass through a silica membrane under pre-

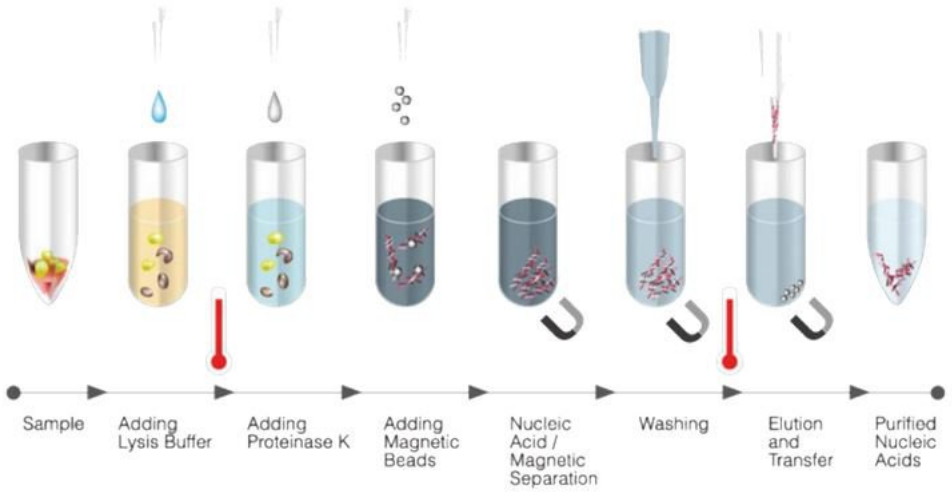

Figure 2.2: Nucleic Acid Extraction Using Magnetic Beads. From Biosan (2021)

defined conditions where they bind, while other impurities pass through (Wikipedia contributors (2021c)). Nevertheless, this repeated centrifugation introduces stress and shear forces on the target molecules, which damage the nucleic acids and most of them are lost resulting in a very poor yield. It also requires a large amount of sample. Thus, it is not at all apt for the PoC devices which have less sample concentration yet, demand higher yield. This brings us to the more efficient method of extraction of nucleic acids using magnetic beads.

In the magnetic bead extraction process, silica coated superparamagnetic beads are used instead to bind the DNA or RNA to the surface of these magnetic beads. While the beads are held immobilized on one side of the plastic vial with the help of an external magnetic force, the other impurities are washed away until only the beads with the nucleic acids bound to them are left behind.Then in the elution step, the nucleic acids are separated from the magnetic bead surfaces and isolated successfully. The major advantage of using magnetic beads is that the yield is much more than the spin column method. The nucleic acids isolated using this method are much more concentrated and thus, allows increased specificity when it comes to capturing

positive or negative test results based on the presence of a viral RNA in a human sample. Moreover, there is no loss or damage of nucleic acids either, allowing for increased sensitivity.

2.3 Composition of the Beads

The beads under consideration for this thesis project are Dynabeads^{TM} MyOne^{TM} Silane from Thermo Fisher Scientific and SPHERO^{TM} Carboxyl Cross-linked Magnetic Particles from Spherotech.

The magnetic core inside the dynabeads is a mixture of two iron oxides maghemite (gamma-Fe_2O_3) and magnetite (Fe_3O_4), which is placed inside the bead matrix by an additional thin polymer shell. Dynabeads are superparamagnetic in nature due to their extremely small size of 1μm diameter. When ferromagnetic multi-domain samples of (Fe_3O_4) are reduced in size to less than 40nm, a single-domain superparamagnetic particle is formed. Hence dynabeads are more closely related to ferromagnetism rather than paramagnetism with respect to magnetic properties as When placed in an external magnetic field, they achieve the highest level of magnetization possible for that specific material and size much like a ferromagnetic material, as all the single-domain magnets align all their magnetic moments in the same direction (antibodies online.com (2021)). Nevertheless, because of being single-domain particles, they do not have as high susceptibility as ferromagnetic materials. On the other hand, they have one common feature like paramagnetic materials as in they also do not retain magnetism when the external influence is removed. The absence of magnetic memory make them extremely effective for magnetic separation of cells or bio-molecules.

The properties of the MyOne Silane Dynabeads were as follows: diameter 1 μm; monodispersity 0.02 um SD, 2% CV; specific surface area varying between the range of 8-16 m^2/g DS and density 1.8 g Ds/cm^3. As the dynabeads are superparamagnetic in

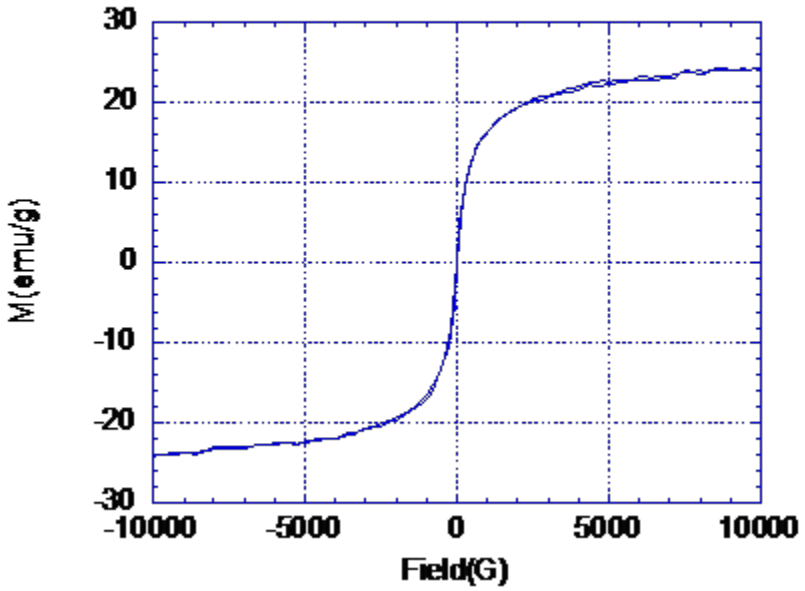

Figure 2.3: Magnetization Curve of Dynabeads (Graph 1)

nature, they have zero values for remanence and coercivity.The magnetization curve of dynabeads have been shown in figures 2.3 and 2.4.

Magnetic susceptibility is a measure of how much magnetized the beads will be in presence of an external magnetic field. It is denoted by χ and is given by the following equation:

$$M = \chi H \tag{2.1}$$

where M stands for the magnetic moment per unit volume and H denotes the field intensity of the magnetic field applied. Paramagnetic materials usually have χ values greater than 0 as is evident because it is 1.4 for dynabeads.Saturation magnetization on the other hand refers to the maximum magnetic field that may be generated by the magnetic beads. More the iron content of the beads, more will be the saturation magnetization. The high saturation magnetization of the dynabeads with a value of 43 kA/m enables a quick and efficient separation even in viscous samples. Dynabeads

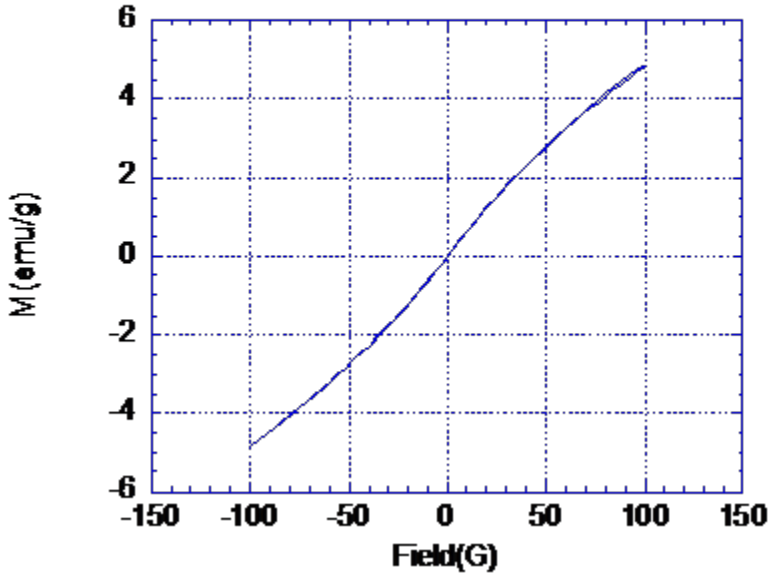

Figure 2.4: Magnetization Curve of Dynabeads (Graph 2)

have an iron content of 26%.

The second type of beads used were the cross-linked magnetic microparticles purchased from Spherotech, spherical in shape with an outer coating of iron oxide and polystyrene onto monodispersed, polystyrene core particles. Though these are also polystyrene polymers with magnetite polymerized to the surface, the cross-linked paramagnetic beads had greater surface area and higher iron content as compared to generic polystyrene magnetic particles sph (2021a). The iron content of the beads vary from 10% to 15% of the particle. These beads are perfect for molecular biology applications like extraction and isolation of nucleic acids, cell separation and applications related to immunoassay reagents sph (2021b).

In the PoC device, in order to detect the presence of SARS-CoV-2 virus, after the extraction process, the nucleic acids need to be mutiplied into millions of copies using the Reverse Transcription-Polymerase Chain Reaction (RT-PCR). The last step of

RT-PCR method is denaturation which occurs at a high temperature of 95 degrees Celsius. Thus, we had a concern whether the paramagnetic beads would function properly inside the testing kit.The melting point of polystyrene is 270 degrees Celsius while its glass transition state is around 100 degrees Celsius. The melting point of cross-linked polystyrene polymers will be more than these. Magnetite also has a high melting point of 2905 degrees Celsius and its Curie temperature is as high as 580 degrees Celsius.Keeping in mind the above figures, we can safely state that the above-mentioned carboxyl coated spherical paramagnetic beads would be a perfect fit for the extraction process.

In conclusion to this chapter, it is important to mention that the dynabeads and the carboxyl-coated cross-linked magnetic beads had one basic difference in their chemical structure as they are superparamagnetic and paramagnetic repectively. The meanings of these two terms and detailed information about the different types of magnets used in this thesis have been mentioned in the following chapter.

Chapter 3

BACKGROUND ON THE MAGNETS

3.1 Permanent Magnets

It is believed that even though all materials have magnetic forces produced inside them, not all of them can be made magnetic. It depends a lot on the atomic structure of the materials. When an electron spins around the nucleus of an atom in an orbital structure, it generates one type of magnetic moment which is known as the orbital magnetic moment. There is a second kind of magnetic moment too which is due to the spin of the electrons. We know that the atomic structure of elements is such that electrons are usually in pairs with opposite spins. As a result of the opposite spins, the secondary kind of magnetic moments produced cancel each other. Moreover, the orbital magnetic moments are randomly arranged as a result of which, usually in most materials, the magnetic moments cancel each other and they end up having no magnetic properties.(Herbst (1993))

Iron, nickel, cobalt are some of the elements which have lone electrons in their atomic structures and thus, their magnetic moments are not cancelled off entirely.

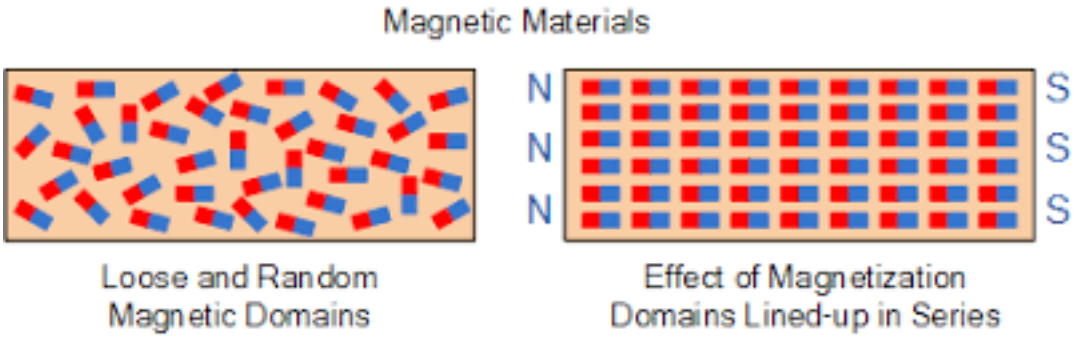

Figure 3.1: Alignment of Random Magnetic Domains in Presence of External Magnetic Field. From ElectronicsTutorials (2013)

These elements thus have a net magnetic moment which make them magnetic in nature. It has been mentioned earlier that the orbital magnetic moments are arranged randomly. When an external magnetic force is applied, these magnetic moments tend to align themselves so that they are parallel to each other. This alignment of magnetic moments create a magnetic field both inside and outside of the material and this is known as magnetic induction as shown in figure 3.1.

An unmagnetized ferromagnetic material usually has small regions ranging from 10 micrometers to 1000 micrometers where the magnetic moments are aligned. When the ferromagnetic material is placed under the influence of an external magnetic field, all the other randomly oriented magnetic domains also start aligning themselves and the regions that were already aligned, tend to increase in size. This is where the concept of permanent magnets come into the forefront. If a large reversible field is required to de-align the magnetic moments or in other words, to de-magnetize, then those types of materials are called permanent magnets. Temporary magnets on the other hand, are those which can be de-magnetized by applying a small reversible magnetic field. Sometimes, weak magnets can be de-magnetized simply by shaking them a lot as shaking tend to make the magnetic moments align themselves randomly once again. Heat is another popular way to de-magnetize permanent magnets. Hence, in magnet specifications Curie Temperature is often mentioned specifying the temperature beyond which the magnet will be de-demagnetized.(Herbst (1993))

Based on the magnetic induction behaviour, there are different types of magnetic materials which have been described below.

- Paramagnetic: Paramagnetic materials have more or less a considerable amount of unpaired electrons as a result of which, these show partial alignments and thus have positive magnetization. Paramagnetic materials do not have any magnetic memory i.e. both the values of remnance and coercivity are zero for

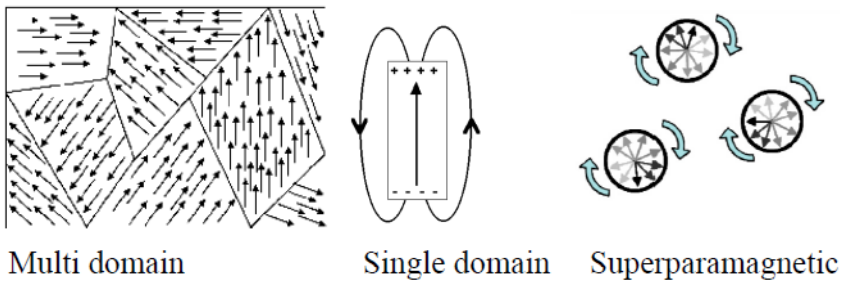

Figure 3.2: Formation of Superparamagnetic Materials from Ferromagnetic Materials. From Ruffert (2016)

such materials. Remnance is the amount of magnetization which is retained by a magnet even at zero magnetic field. Coercivity, on the other hand, is the amount of reverse field applied to demagnetize a magnet. Since paramagnetic materials lose their magnetization as soon as the external magnetic field is removed, hence, they do not need any reverse field to be demagnetized.

- Diamagnetic: Diamagnetic materials have no or few lone or unpaired electrons and thus they show very weak magnetization in presence of external magnetic field. It is very difficult to induce magnetic moment in these type of materials.Diamagnetic materials exhibit negative magnetization.

- Ferromagnetic: Ferromagnetic materials form the strongest permanent magnets as these induce strong magnetic moments in presence of a magnetic field. The atoms are aligned perfectly so that current can flow easily through these materials which make them components of some of the strongest permanent magnets available in the market like iron, nickel, cobalt etc.

- Superparamagnetic materials have characteristics of both ferromagnetic and diamagnetic materials. When ferromagnetic materials with their multidomain structures are reduced to particles of size below 40 nm, they give rise to single-domain superparamagnetic materials as shown in figure 3.2. Because of this

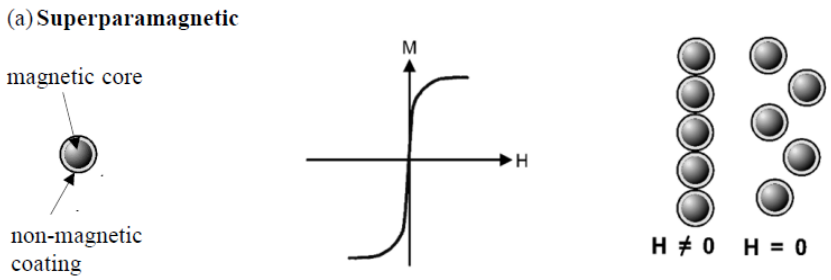

Figure 3.3: Characteristics of Superparamagnetic Materials. From Ruffert (2016)

single domain structure they possess, they align themselves easily under the influence of an external magnetic field, thus attaining the strongest magnetization possible for a particle of that particular size. This strong magnetization property make them similar to ferromagnetic materials. On the contrary, their similarities with paramagnetic materials lie in the fact that even superparamagnetic materials have no magnetic memory in absence of an external magnetic field. Both remnance and coercivity of superparamagnetic materials are zero.

Comparing figures 3.3 and 3.4, it can be observed that when magnetic field intensity, H is zero for ferromagnetic materials, the beads still do not break the straight alignment and continues to retain magnetization. Also, in the hysteresis loop, the demagnetization curve is observed to be tracing back a different path than the magnetization curve, thus making it evident that ferromagnetic materials have both non-zero values for remnance and coercivity. For superparamagnetic materials on the other hand, when H is zero, the beads lose their alignment all at once and start aligning in a random manner. This shows that they lose their magnetization property as soon as the external magnetic field is removed. The hysteresis loop too curves the same path both for magnetization and demagnetization.

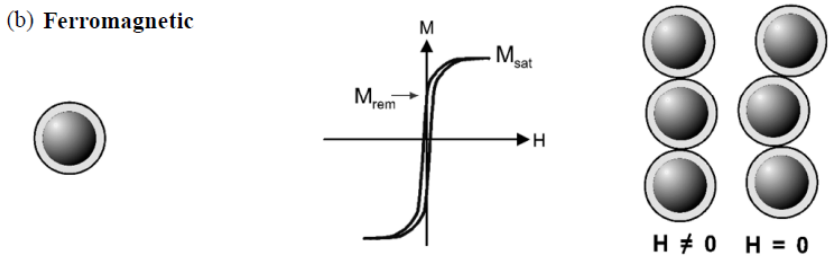

Figure 3.4: Characteristics of Ferromagnetic Materials. From Ruffert (2016)

3.2 Electromagnets

The other type of magnets which can be used to manipulate the movement of magnetic beads is an electromagnet. Electromagnetism follows the basic principle of generating a magnetic field around a coiled wire when current is passed through it. The advantage of using electromagnets over permanent magnets, particularly when it comes to application in point-of-care devices are as follows:-

- The magnetic strength of electromagnets can be manipulated based on the current passed through the circuit.
- They can be turned on and off at rapid intervals of time using electrical signals

The disadvantage of electromagnets, on the other hand, with respect to permanent magnets is that their magnetic strength is usually weaker when compared to the permanent magnets, as will be seen in the experiments discussed in the following chapters.

3.3 Other Parameters Determining Magnetic Strength

There are a few parameters like the Maximum Pull in lbs. and the Maximum energy product which are two more factors affecting the magnetic strength of a permanent magnet along with the magnetic flux density.

The force which is required to pull a magnet away from a steel object or another magnet is determined by the maximum pull. More the maximum pull value, stronger will be the magnet. On the other hand, maximum energy product is the quantity which denotes the maximum magnetic field that the magnet can produce. Larger is the value of the product, greater will be the potential for reducing the size and weight of a permanent magnet. It is given by BH_{max}. In the experiments with the different permanent magnets, it will be noticed that two ceramic magnets with same values of magnetic flux densities have different magnetic strength overall, because of the difference in values for these two parameters. So, when we use a permanent magnet for attracting the magnetic beads, it is necessary that we keep these two factors in consideration too.

Chapter 4

LITERATURE REVIEW

In this chapter, we have touched upon the concepts mentioned in a few research papers regarding the manipulation of magnetic beads and how they might be integrated into the MEMS devices.

4.1 BioMEMS Chip with Integrated Micro Electromagnets

Integrating electromagnets in integrated circuits and microfluidics is a challenging field of research but a very promising one nevertheless. Due to lack of reliable techniques of proper fabrication of chips, it is still not an established alternative yet. The type of devices which exist right now are usually microcapillary channels embedded on a chip while the external electromagnets are placed outside or an integrated chip with electromagnetic features combined with post-fabricated microfluidic structures.

In the paper by Zheng *et al.* (2014), the design of a BioMEMS chip is proposed however, which would manipulate magnetic particles like the beads, by integrating a planar microcoil array along with a microcapillary structure within a single chip. The planar microcoil array had been chosen because of its ability to control the magnetic field by varying the current flowing through the microcoil structure and also because it is found to be more compatible with how microfabrication works in practical terms. The geometry of individual microcoil designs had to be investigated for specific applications due to which, four microcoil array geometries have been studied in this paper. Before the geometries are discussed though, the basic principle based on which the microcoil array was designed needs to be addressed first.

4.1.1 Principle of Microcoil Array Design

When an external magnetic force is applied on the magnetic beads, the force on the magnetic beads are given by the following Maxwell equation:-

$$\vec{F_{mag}} = V\chi_m(\vec{H}.\nabla)\vec{B} \tag{4.1}$$

where $\vec{F_{mag}}$ denotes the magnetic force on the beads, V is the volume of bead, χ_m is the magnetic susceptibility per unit volume, $\vec{H}$ is the magnetic field intensity and $\vec{B}$ is the magnetic flux density. The relationship between $\vec{B}$ and $\vec{H}$ is again given by $\vec{B} = \mu\vec{H}$, where μ is the permeability of the medium. This relation proves that the magnetic force on bead not only depends on the magnetic field intensity but also on the magnetic field gradient.

Finally, it is inferred that if a spiral microcoil has multiple turns of concentric square loops with differential lengths, according to Biot-Savart law, the total magnetic field exerted will be the sum of the magnetic field induced by each loop. This is the shown in the following equation:-

$$\vec{B} = \int d\vec{B} = \int \frac{\mu_0}{4\pi}.\frac{Id\vec{l} \times \vec{r}}{|r|^2} \tag{4.2}$$

where μ_0 is the magnetic constant, I is the total current passing through the coil, $d\vec{l}$ is the differential length of the wire in the same direcrion of the current, $\vec{r}$ is the displacement unit vector, having a direction which points from the wire element to the point at which the magnetic field is being computed and r is the distance between the wire and that point of computation. The above equation shows that the magnetic flux density $\vec{B}$ is directly proportional to the current passing through the coil but it has an inverse relationship when it comes to the size of the coil or more specifically, its diameter. As the coil size is reduced, less current will be required to generate the magnetic field and thus, for fabrication minimum metal width would

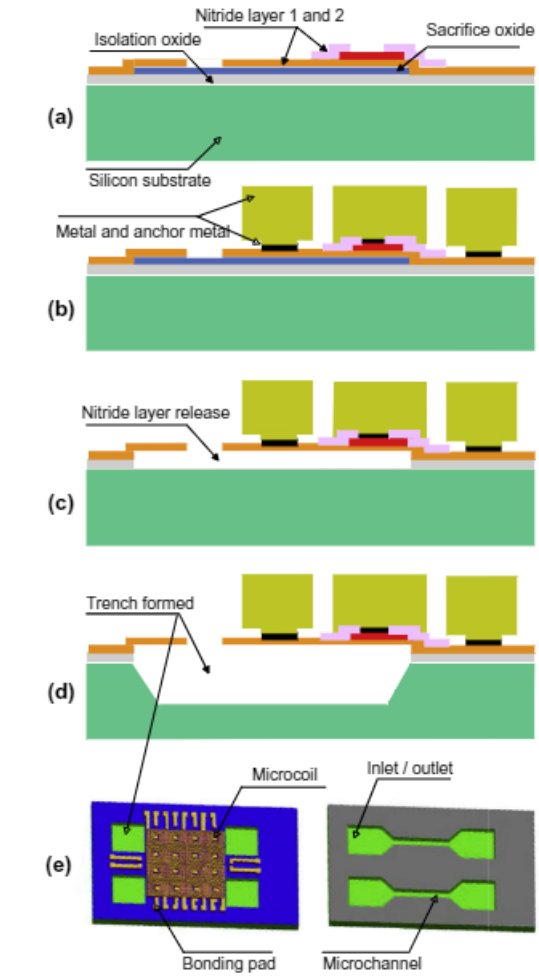

Fig. 1. Main fabrication flow used in this design: (a) deposition and pattern of isolation oxide, sacrifice oxide and nitride layer 1 and 2; (b) deposition and pattern of metal layer(coil structure), anchor metal layer(connection between polysilicon and metal) and polysilicon layer; (c) removal of oxide layer by HF solution to form the suspended structure; (d) KOH silicon etching to form the trench; (e) topview of final device model in Coventorware to show the whole device and microchannel.

Figure 4.1: Fabrication Steps for the Bio-MEMS Chip. From Zheng *et al.* (2014)

end up generating the strongest magnetic field. Using this concept in mind, the chip was designed as shown in figure 4.1 using MetalMUMPs process of fabrication.

4.1.2 Magnetic Field Strength Required to Attract Magnetic Beads

Once the geometry and the fabrication process of the microcoil array were fixed, the next question which needed to be asked is the magnetic field strength required to attract the beads. In order to attract the beads and hold them steadily, the magnetic

force should balance or be greater than the hydrodynamic force of the beads. The magnetic beads when placed under the influence of an external magnetic field not only experiences the magnetic force, but also the hydrodynamic and gravitational forces. Due to the micrometer size of the beads, the gravitational force is often neglected. Following Stoke's Law, it is known that the hydrodynamic force can be given by the equation:-

$$\vec{F}_{hydro} = 6\pi\eta R_{bead}(\vec{v}_{bead} - \vec{v}_{fluid}) \tag{4.3}$$

In the above equation, $\vec{F}_{hydro}$ is the hydrodynamic force on the magnetic beads, R_{bead} is the radius of the magnetic bead, η is the viscosity of the fluid, $\vec{v}_{bead}$ and $\vec{v}_{fluid}$ are the velocities of the particle and the fluid medium respectively.

Based on all these calculations, a BioMEMS chip was designed with a current consumption of 40 mA generating a magnetic field stronger than 10 Gauss on the plane. One disadvantage of this design as mentioned in the paper is that it was not found suitable for smaller microchannels as the pressure would not be high enough to overcome the surface tension of water.

4.2 Co-fabricating Electromagnets and Microfluidic Systems in PDMS Channels

In the paper by Siegel *et al.* (2006), microfabrication of electromagnets and microfluidic channels are discussed with respect to embossing in PDMS which stands for polydimethylsiloxane.

While derivating the time required to move a superparamagnetic bead across a microfluidic channel, it is mentioned in the paper that, two types of forces act on the superparamagnetic beads under consideration which are the magnetic force denoted by F_x and the Stokes Force denoted by F_s. Keeping in mind that the product between mass and acceleration of a particle equals the force applied on it, the following equation can be written for the balance of forces acting on the magnetic beads in x-

direction:-

$$ma = F_s + F_x \tag{4.4}$$

Neglecting the inertia of the magnetic bead i.e. ma=0, the equation can be modified as:-

$$0 = 6\pi\eta R_v - V\chi\mu_0 \frac{{I_{wire}}^2}{2\pi^2 x^3} \tag{4.5}$$

Considering the magnetic beads move towards the electromagnet which is the negative x-direction for the study, the equation can be simplified to as follows:-

$$V\chi\mu_0 \frac{{I_{wire}}^2}{2\pi^2 x^3} = 6\pi\eta R(-\frac{dx}{dt}) \tag{4.6}$$

Separating the independent variables in the above mentioned equation and writing the volume of the beads in terms of radius, the equation can be written as:-

$$\frac{1}{9}\frac{\chi\mu_0}{\pi^2\eta} R^2 {I_{wire}}^2 dt = -x^3 dx \tag{4.7}$$

Integrating both sides of the equation from initial position of the magnetic bead, which has been denoted as 'b' in this paper, to the sidewall of the microcapillary channel, 'a' the equation can be written as:-

$$\frac{1}{9}\frac{\chi\mu_0}{\pi^2\eta} R^2 {I_{wire}}^2 \int_0^{t_{cap}} dt = -\int_b^a x^3 dx \tag{4.8}$$

$$t_{cap} = \frac{9}{4}\frac{\pi^2\eta}{\chi\mu_0 R^2}\frac{b^4 - a^4}{{I_{wire}}^2} \tag{4.9}$$

This gives us the time required to move a superparamagnetic bead across a microcapillary channel.

Chapter 5

EXPERIMENTAL SETUP

In this project, the initial aim was to design an electromagnetic circuit which would have attracted the magnetic beads, Dynabeads MyOne Silane from ThermoFisher Scientific to be specific, so that instead of using a permanent magnet, we can incorporate an electromagnetic circuit within a point-of-care diagnostic device. As mentioned in Chapter 2, magnetic beads are an essential component for any point-of-need testing kit. But in order to attract them, we can either use electromagnets or permanent magnets as mentioned in Chapter 3.

The initial experiments were thus based on some random design plans for developing an electromagnetic circuit with varying voltage and current, which would eventually serve our purpose.

5.1 Experiments on Designing Electromagnetic Circuits

5.1.1 Experiment with Electronic Wire and Metal Core

The first experiment consists of two random setups trying to create a strong enough magnetic field to attract the beads in the solution. At the time of this experiment, the magnetic strength required to attract the dynabeads was unknown.

- Experimental Setup 1: Electronic wire had been coiled multiple times on a small metal core and connected to the power supply. This setup created a strong magnetic field around it, which attracted the beads within 1 to 2 minutes on the magnet facing side of the plastic vial. As the orientation of the vial was kept on changing with respect to the electromagnet setup, the beads continued

to move and accumulate along the field lines. Even after removing the vial away from the circuit, the beads did not disperse instantly and were held together for enough time, as is desired.

Observations: Voltage applied was 1.5V, current consumed was 5 amperes and number of turns were unknown.

Discussions: The core around which the electronic wire had been wrapped was a really small one as a result of which,the wire had to be coiled in layers. Current of 5 amperes and voltage of 1.5 volts were too high with respect to a small point-of-care diagnostic device. Both the voltage and the current needed to be scaled down. Hence, this setup was not a perfect circuit for our requirements.

- Experimental Setup 2: Six small metal cores were placed inside the plastic holder around which an electronic wire was kept coiled, hoping that it would generate a magnetic field in the center. The vial was dropped in the center of the plastic holder. It did create a magnetic field but not strong enough to hold the beads in a steady position. The entire setup took a lot more time to attract the beads as compared to the previous experimental setup. The experimental setups are depicted in 5.1 and 5.2

  Observations: Voltage applied was 6.18V, current consumed was 3.56 amperes and number of turns were unknown.

  Discussions: Coiling the wire around a plastic holder was not a convenient method of design as when current passes through the wire, it tends to heat up and plastic holder might melt in presence of heat. Current consumption and voltage applied were still quite high with respect to our needs for the point-of-care device.

Figure 5.1: Experimental Setup Showing Supply Voltage as 6.18 Volts and Current as 3.56 Amperes

5.1.2 Experiment with Beat Frequency Oscillator

In this experimental setup, a three-stage Beat Frequency Oscillator circuit with its frequency mixing technique was used to characterize the bead concentration in a given sample. In an attempt to scale down the current and voltage requirements of the electromagnetic circuit,certain alternative circuits were being explored, one being the Beat Frequency Oscillator (BFO) circuit. It was believed initially that there were two possible ways for influencing the movement of the magnetic beads- one being the use of strong magnetic field to apply magnetic force on the beads. The second one was to measure the changes in the magnetic flux by measuring the inductance variation. The BFO was supposed to be implementing the second method.

Figure 5.2: Experimental Setup Showing the Multimeter Reading for the Current

Beat frequency oscillator is a type of radio frequency oscillator circuit which generates a constant sine wave of a particular frequency called the BFO frequency denoted by f_{BFO}. The signal frequency of the receiver is known as an intermediate frequency and is denoted by f_{IF}. The principle of operation of a beat frequency oscillator circuit depends on the mixing of these two signals as the two frequencies are added and subtracted in the detector resulting in the beat frequency which generates a tone in the speaker of the receiver.The equation is given as $f_{audio} = |f_{IF} - f_{BFO}|$. (Wikipedia contributors (2021a))

Figure 5.3 shows the beat frequency oscillator circuit used for this experiment. The two blue radial dipped inductors (L1, L2) together with ceramic trimmers (CV1 and CV2) set the frequencies of the two Clapp oscillators. They are mixed in Q1 and

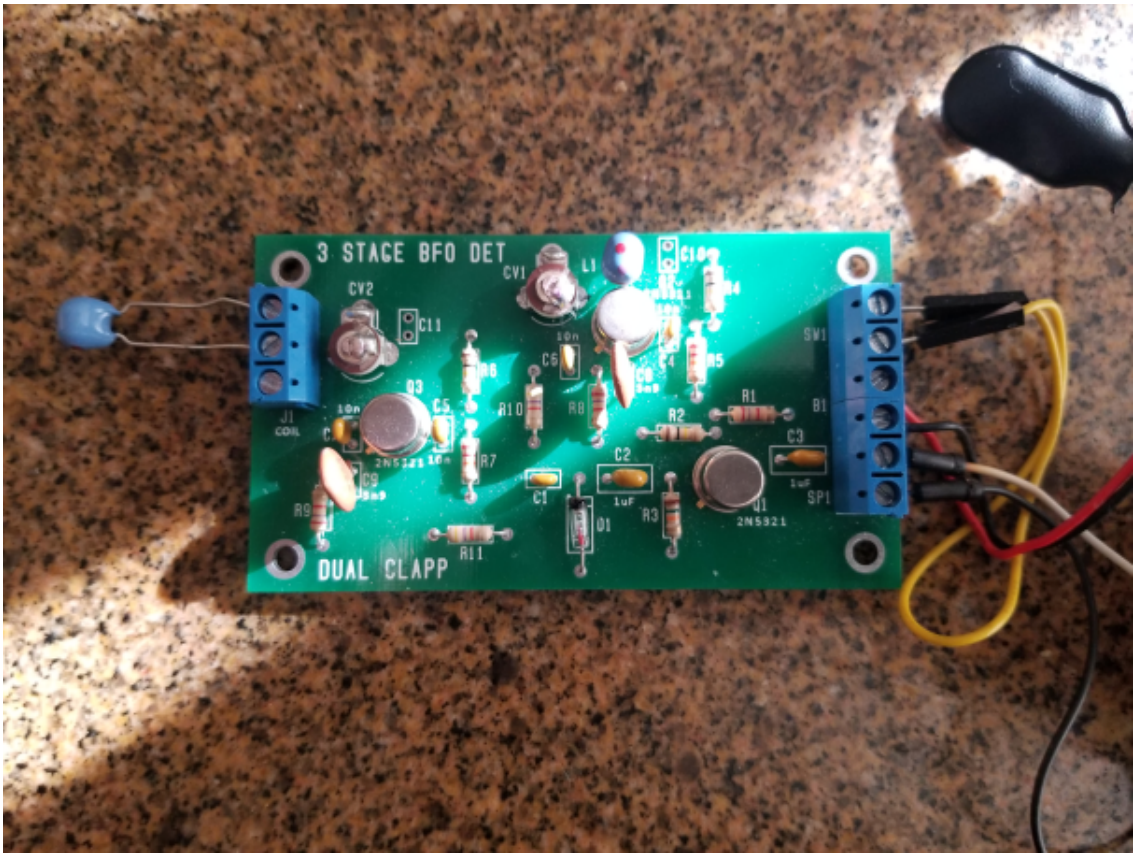

Figure 5.3: Three Stage Beat Frequency Oscillator Circuit Used for the Experiment

the products would go to an oscilloscope, preferably with an FFT function to look at the frequency components. Figure 5.4 depicts the initial setup for the experiment with the two blue inductors kept intact in the BFO circuit.

Replacing the blue inductor coil screwed into J1, with a coil around the vial containing the magnetic beads, the mixing products on the output should have been observed. Two mixed frequencies would show products that shift on an oscilloscope in the presence of beads. The amount of frequency shift should be relative to the number of beads present inside the vial or in other words, to the magnetic bead concentration. The principle of operation lies in the fact that when the coil around the vial with the magnetic beads inside it, was connected at the place of the inductor J1, the magnetic flux changed due to the beads. The flux is subject to convergence or in this case,

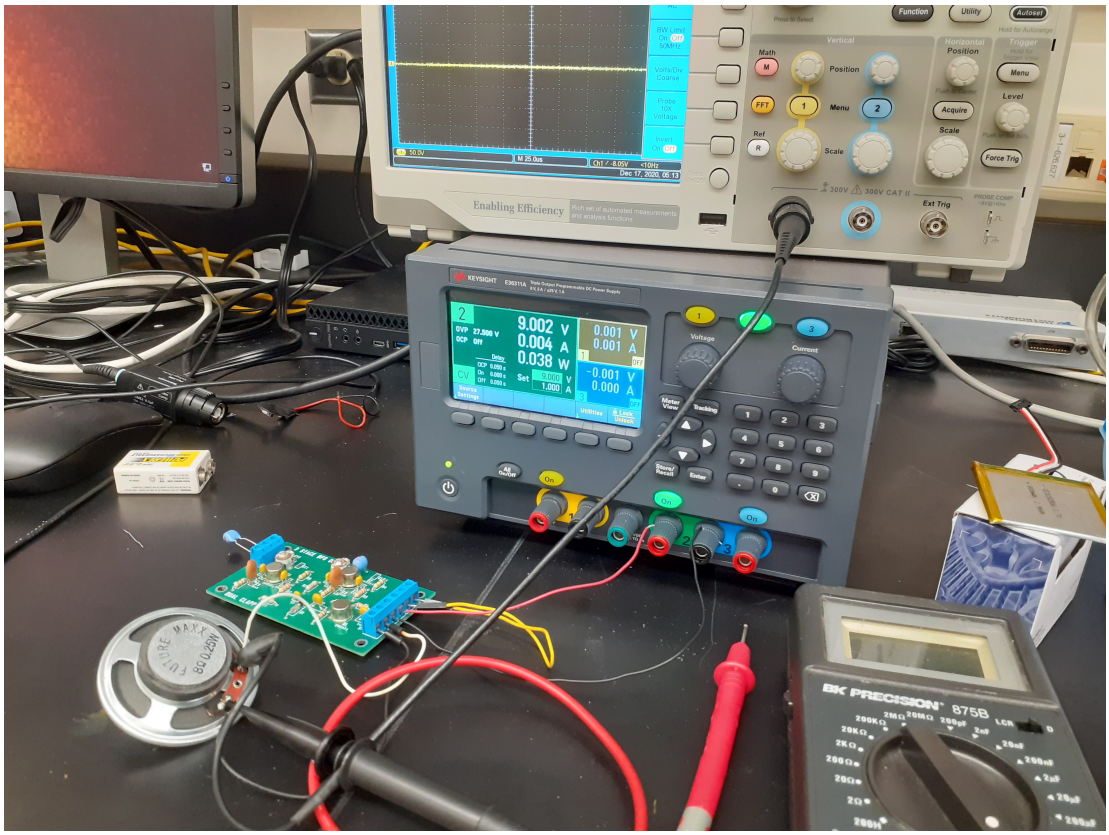

Figure 5.4: Initial Setup with the Two Blue Inductors in BFO Circuit

concentration of the beads. The more the beads inside the vial, the higher the flux concentration will be and so the higher the inductance of any coil around the plastic vial. This then leads to a change in the mixing frequency products. As a result, it does not require huge current flow when it is really the inductance change that is being monitored and magneto-motive force and hence high current draw is not being used to attract the beads. Looking at the change of magnetic flux due to the presence of the beads should allow one to determine how many beads are in the solution by looking at frequency shift amounts.

In this experiment, we observed a frequency shift in the harmonics every time we replace one of the inductors with a different vial. First, we replaced it with a wired coil with nothing inside it but air as shown in figure 5.5. In the next setup as

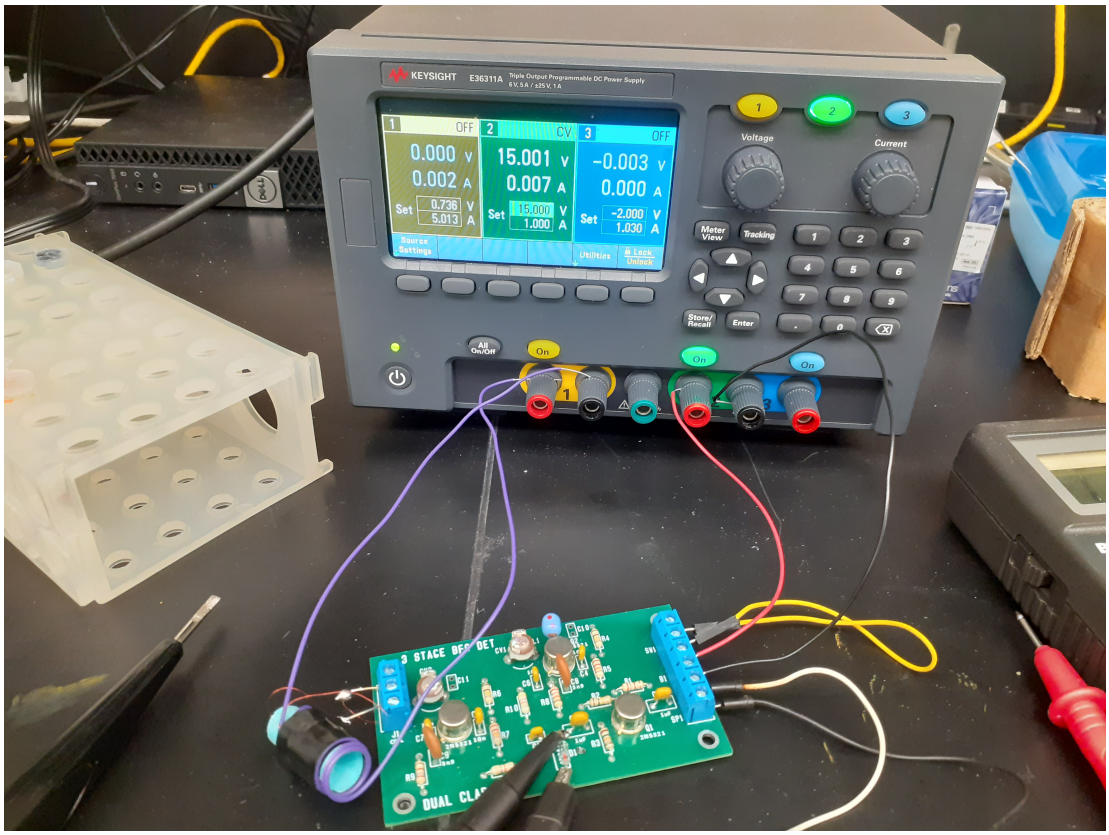

Figure 5.5: Left Blue Inductor Replaced with a Wired Coil

shown in figure 5.6,a vial containing the dynabeads was placed inside the coil which again showed a significant shift in the harmonic frequency though the fundamental frequency remained the same. The last two setups were with a vial of diluted magnetic beads in water and another one with only placed inside the coiled wire. The frequency shift of the harmonic was a measure of the changing magnetic flux due to the presence of different substances within the coil- sometimes magnetic beads, sometimes air and sometimes water.

The frequency shifts corresponding to each setup has been documented in the table 5.1.Figure 5.7 shows the frequency readings of the fundamental and its harmonic corresponding to the setup shown in 5.6.

This experiment was indeed a measure of the number of magnetic beads present

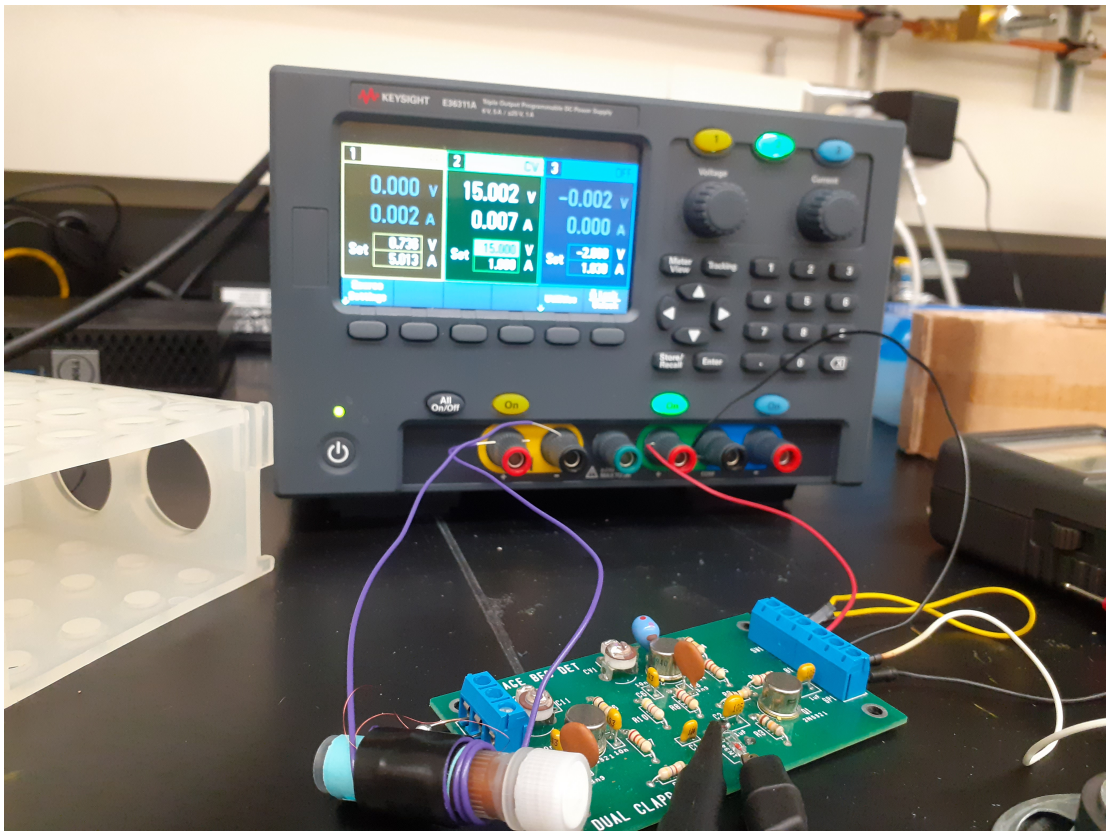

Figure 5.6: Left Blue Inductor Replaced with Vial of Dynabeads

Experimental Setup	Frequency of Fundamental(Hz)	Frequency of Harmonic(Hz)
Air inside Coiled Wire	21.83	217.39
Dynabeads inside Coiled Wire	21.83	200
Dynabeads diluted in water inside coiled wire	21.83	113.64
Water inside Coiled Wire	21.83	96.15

Table 5.1: Frequency Shifts of the Harmonic in Different Experimental Setups of the BFO Circuit

Figure 5.7: Harmonic Shifted to 200Hz for the Setup with the Dynabeads Inside the Vial

as a function of the changing magnetic flux and thus, the frequency shift, but it was in no way related to what was required for the development of an electromagnetic circuit for the PoC device. It was not possible to characterize any other parameter of the magnetic bead excepting its concentration with this experiment and hence, alternate circuits had to be considered.

5.1.3 Experiment with the Solenoid

In the next experiment, a solenoid was built using magnet wire and iron rod.The magnet wire was wound 1410 times around the core which was a 6 inches long soft iron rod with diameter of 0.5 inches. The copper coating on the two ends of the magnet wire were scraped off and connected to the power supply.

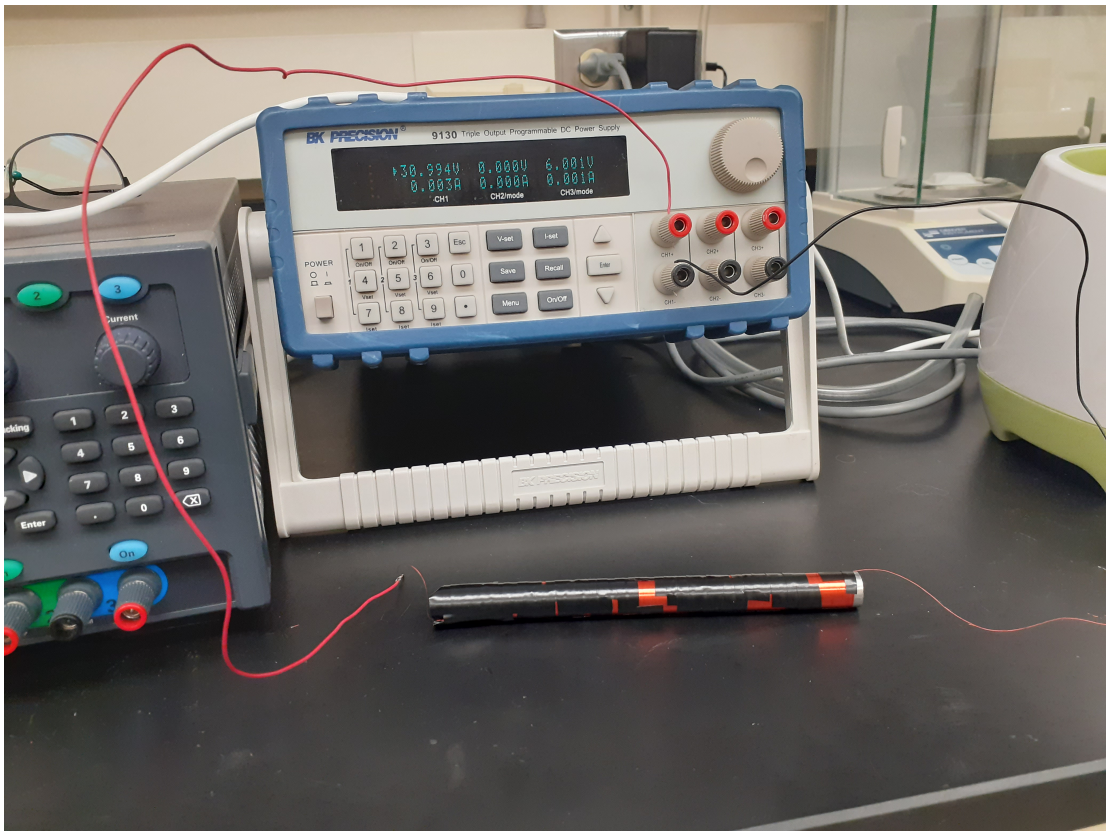

Figure 5.8: Experimental Setup of Solenoid Built with Soft Iron Core and Magnet Wire

Initially, a voltage of 6 volts had been applied which did not create a magnetic field. As we kept on increasing the voltage to 31 volts, the solenoid started heating up very slowly, creating a weak magnetic field around it. The magnetic field created was not strong enough to attract the dynabeads. A picture of the setup has been shown in figure 5.8

5.2 Microscopy Imaging

5.2.1 Compound Microscope

The compound microscope used to capture the images of the different beads was Nikon Eclipse LV100. Compound Microscope is called so because instead of using a

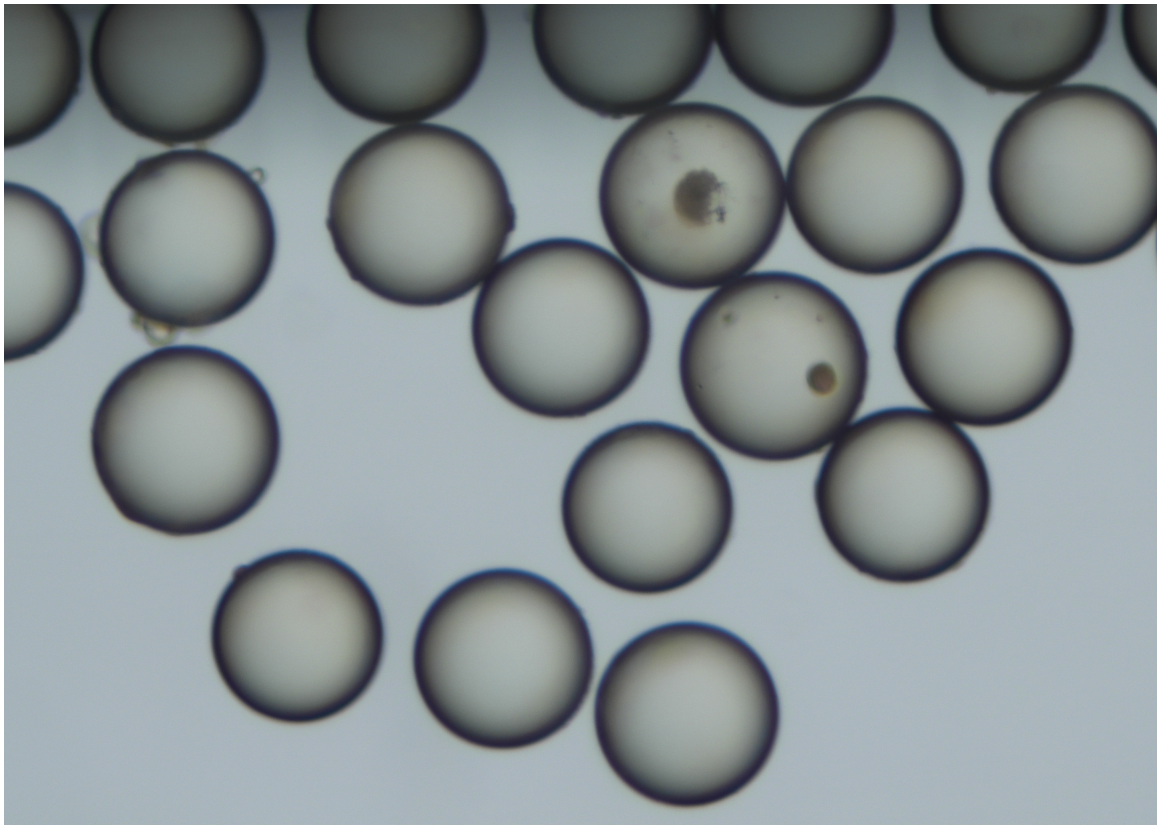

Figure 5.9: CMX-1000-10 of Average Diameter 103.3μm as Captured by Nikon Eclipse LV100

single magnifying lens, it uses multiple lenses to capture the images of the samples. The objective lens of such a microscope is compounded with the eyepiece lens as a result of which higher magnification is achieved (Microscope World (2021)). In the compound microscope used for this project, the highest magnification that can be achieved is 50x.

5.2.2 Phase Contrast Microscope

"Phase-contrast microscopy is an optical microscopy technique that converts phase shifts in light passing through a transparent specimen to brightness changes in the image"(Wikipedia contributors (2021b)).The phase contrast microscope used in this project was Nikon Eclipse TS100 which had a combination of three phases. The main

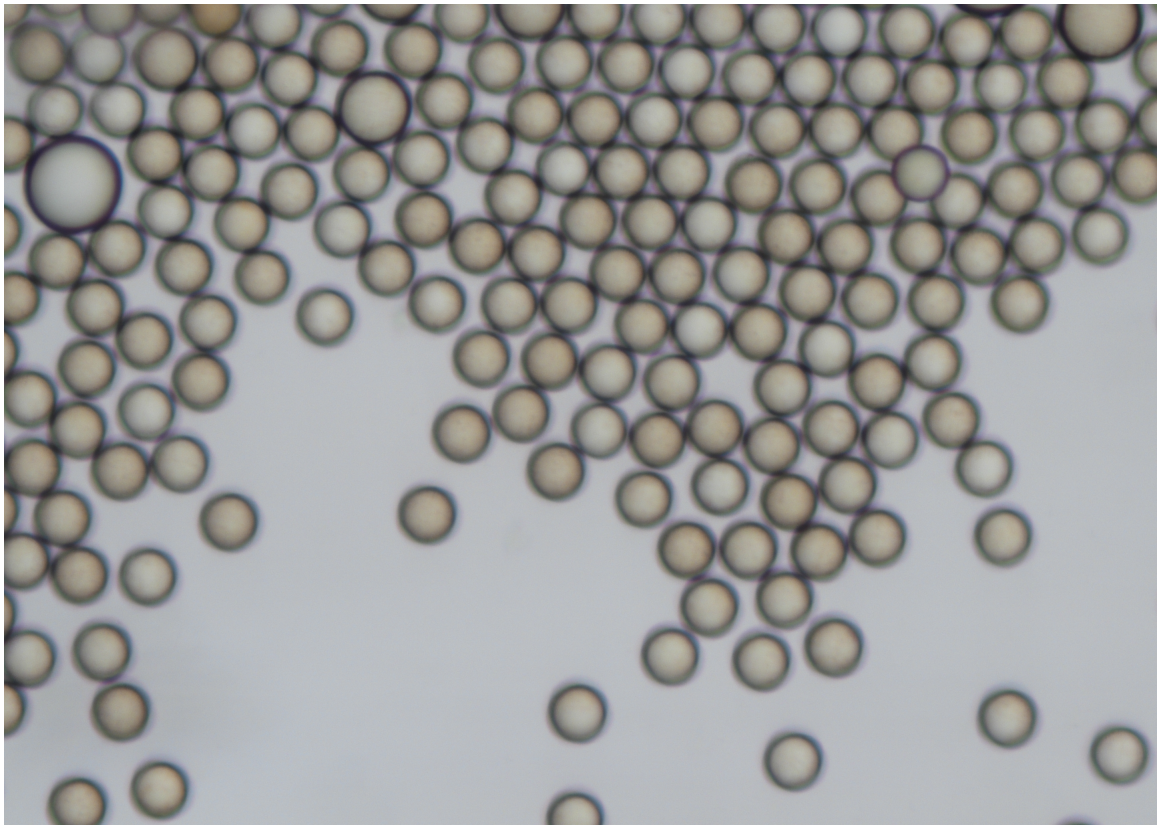

Figure 5.10: CMX-300-10 of Average Diameter 32.2μm as Captured by Nikon Eclipse LV100

objective of using the phase contrast microscope was to observe the inner core of the magnetic beads along with that of the outer coating around the beads. Needless to say, once the phase was adjusted properly both the inner and outer cores were clearly visible for CMX-1000-10 (103.3 um), CMX-300-10 (32.2 um) and CMX-200-10 (18.5 um) beads as shown in figures 5.14, 5.15 and 5.16. Figures 5.17 and 5.18 are the images captured for the smallest sized beads and are not clearly visible by the phase contrast miscroscope.

5.2.3 Dissection Microscope

Though dissection microscope and compound microscope both have binocular eyepiece, there are some significant differences between the two. A dissecting micro-

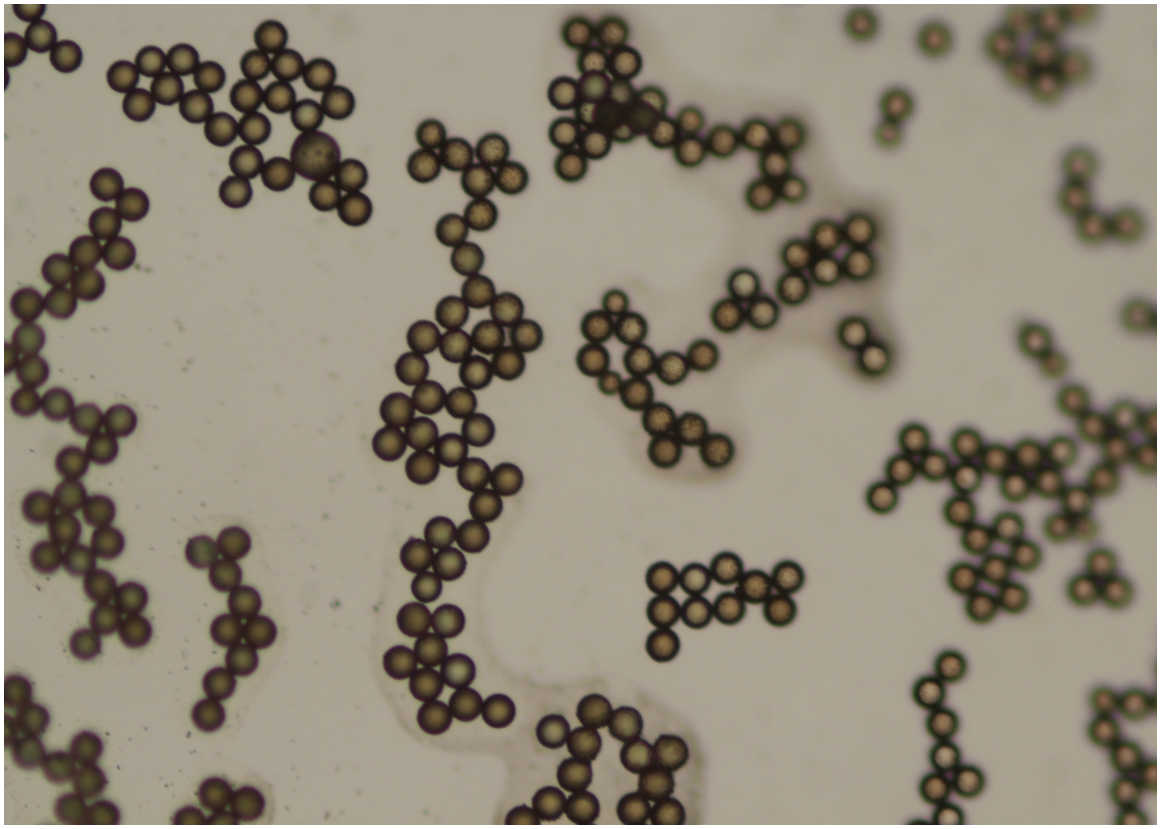

Figure 5.11: CMX-200-10 of Average Diameter 18.5μm as Captured by Nikon Eclipse LV100

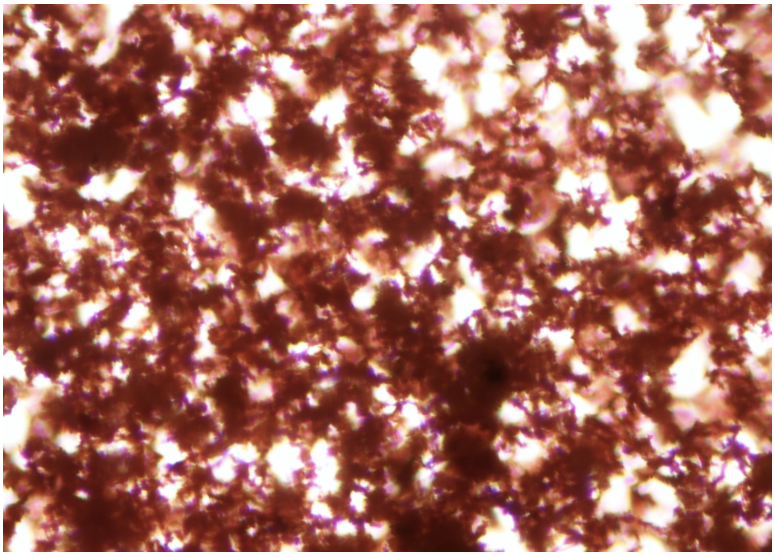

Figure 5.12: CMX-40-10 of Average Diameter 4μm as Captured by Nikon Eclipse LV100

Figure 5.13: CMX-10-10 of Average Diameter 1.17μm as Captured by Nikon Eclipse LV100

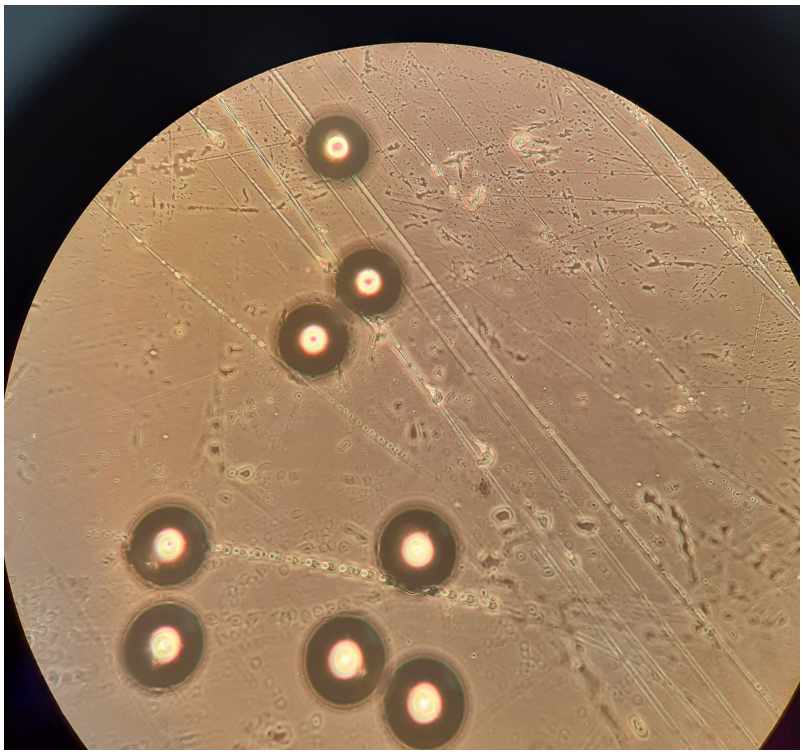

Figure 5.14: CMX-1000-10 of Average Diameter 103.3μm as Captured by Phase Contrast Microscope

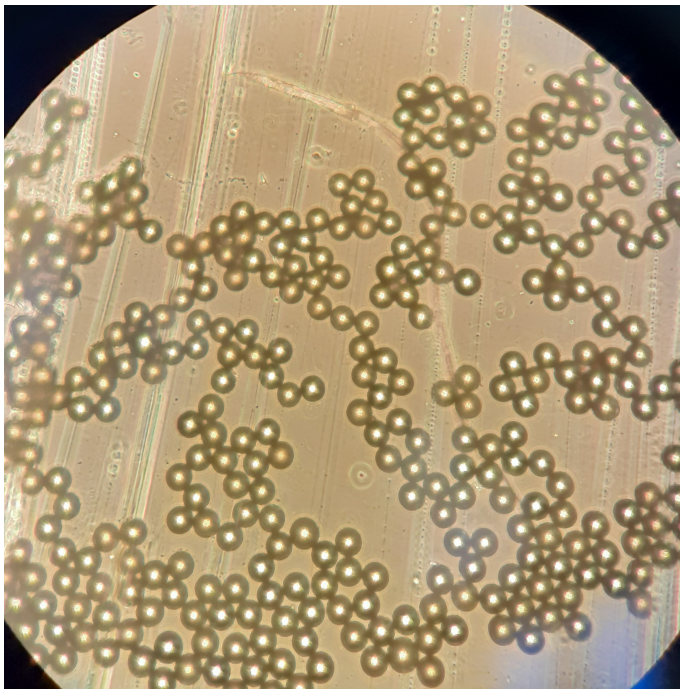

Figure 5.15: CMX-300-10 of Average Diameter 32.2μm as Captured by Phase Contrast Microscope

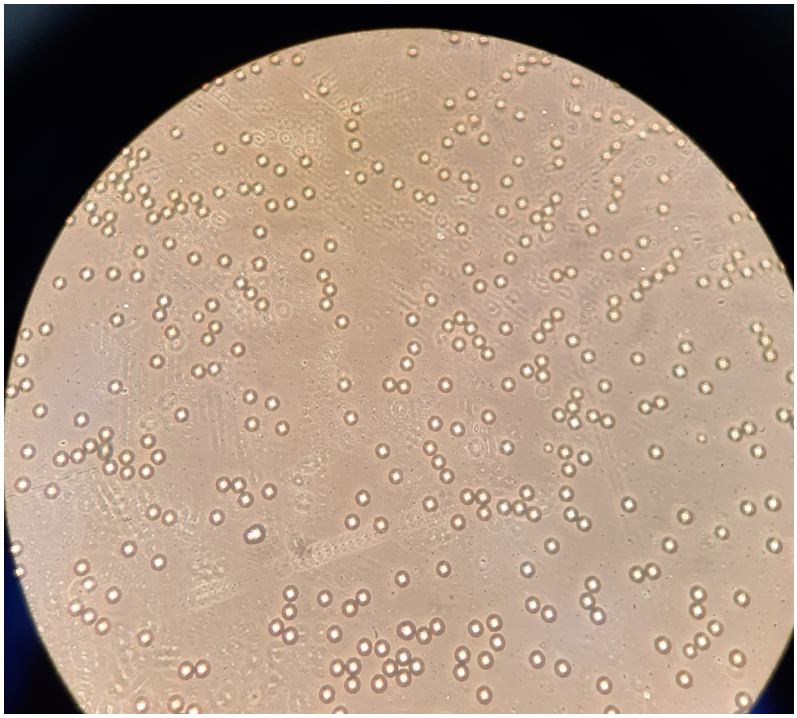

Figure 5.16: CMX-200-10 of Average Diameter 18.5μm as Captured by Phase Contrast Microscope

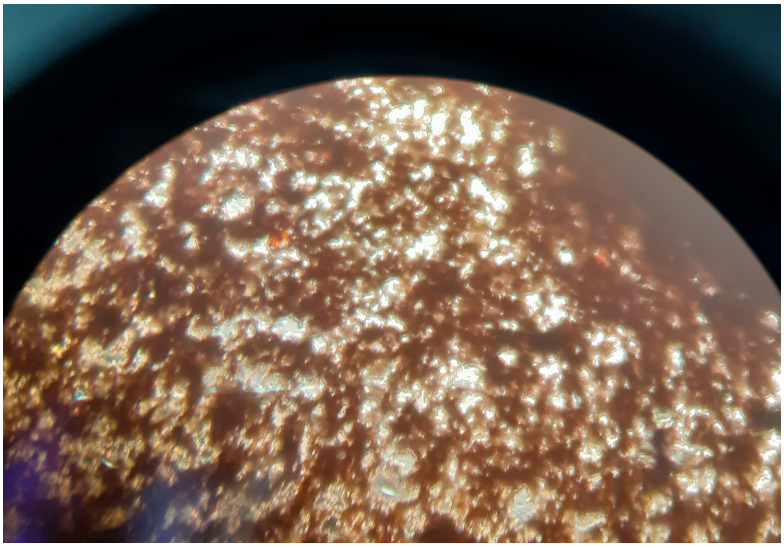

Figure 5.17: CMX-40-10 of Average Diameter 4μm as Captured by Phase Contrast Microscope

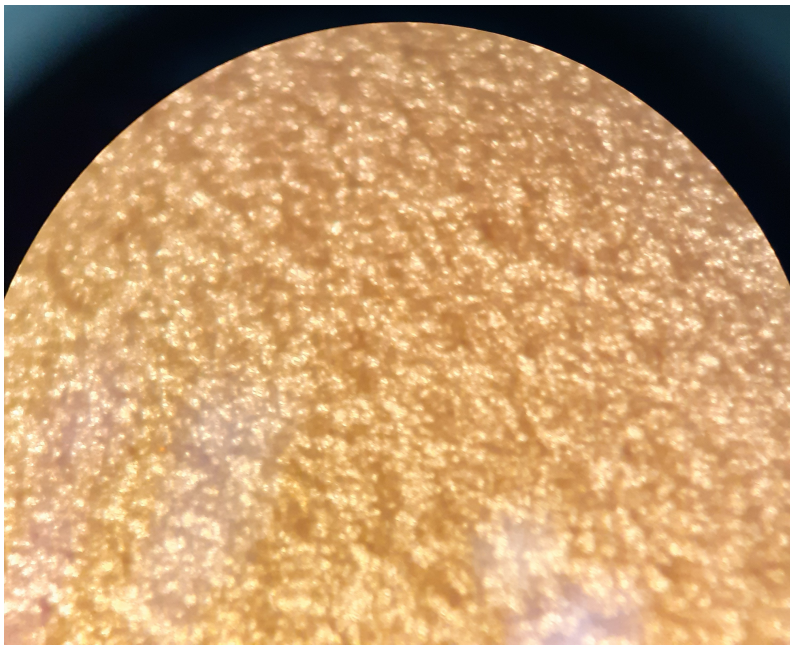

Figure 5.18: CMX-10-10 of Average Diameter 1.17μm as Captured by Phase Contrast Microscope

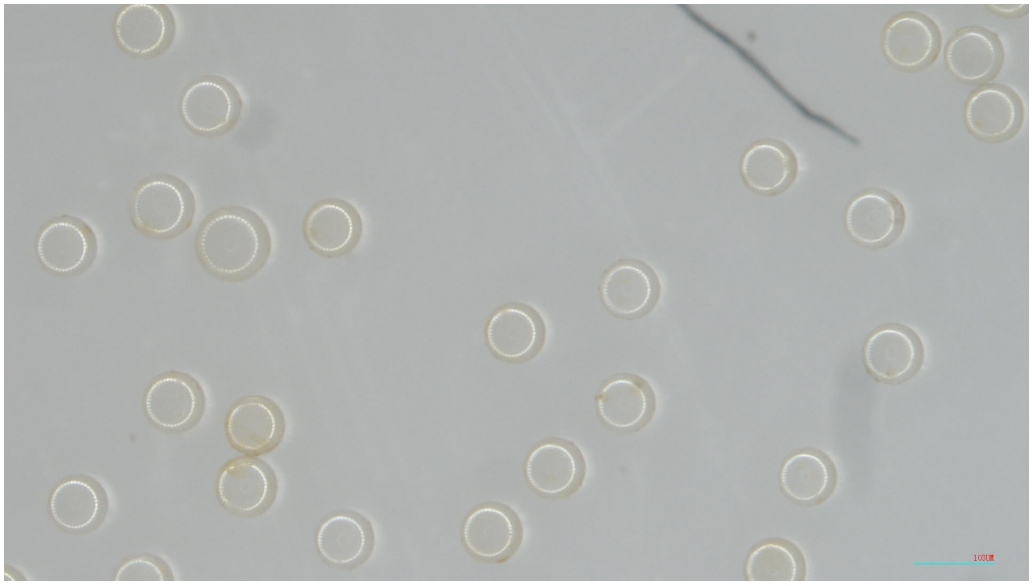

Figure 5.19: CMX-1000-10 of Average Diameter 103.3μm as Captured by Dissection Microscope

scope provides a three-dimensional image "with a discernible depth of field" (Microscope.com (2021)). Since it has the three-dimensional imaging capability, its magnification is usually lower than the compound microscope. As is evident from the figures 5.19, 5.20,5.21,5.22 and 5.23, the images have lower resolution and magnification as compared to those captured by the compound microscope, but on the other hand they have depth, whereas the images captured by the compound microscope are flat and lack depth. The one other advantage it had was that the light shone from above on the workbench which was kind of ideal for the opaque sample and setup we had. It was easier to study the movement of the beads in a microfluidic chip and calculate its velocity keeping a magnet underneath the chip, with this microscope because of this very feature. The dissection microscope used was Nikon SMZ1270 and the camera used was Nikon Digital Sight 1000.

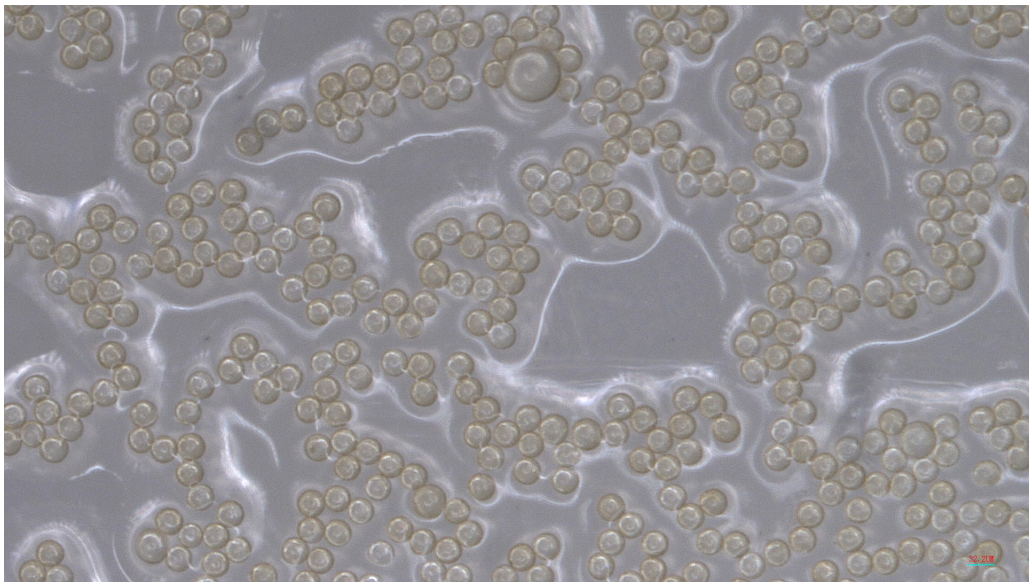

Figure 5.20: CMX-300-10 of Average Diameter 32.2μm as Captured by Dissection Microscope

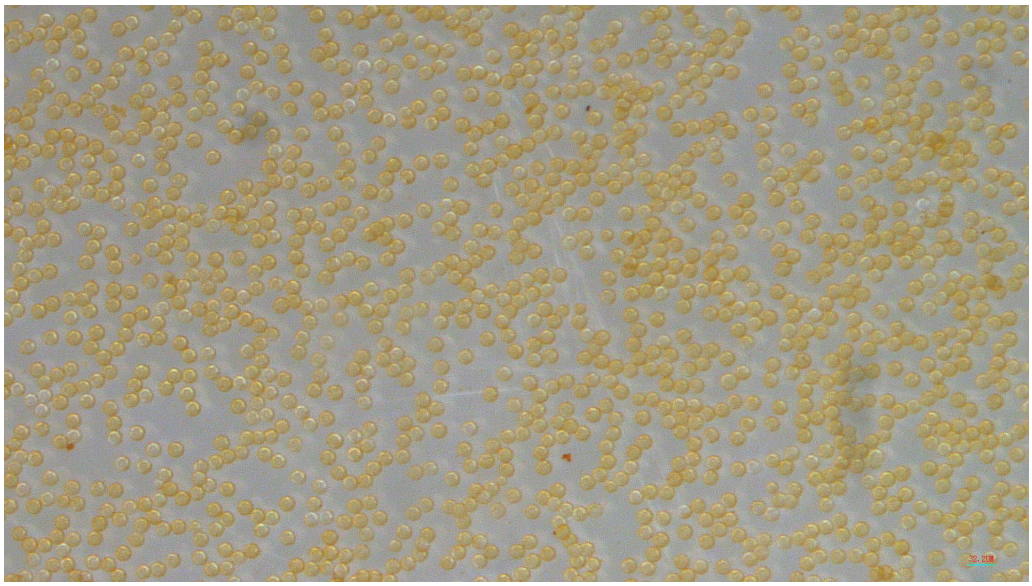

Figure 5.21: CMX-200-10 of Average Diameter 18.5μm as Captured by Dissection Microscope

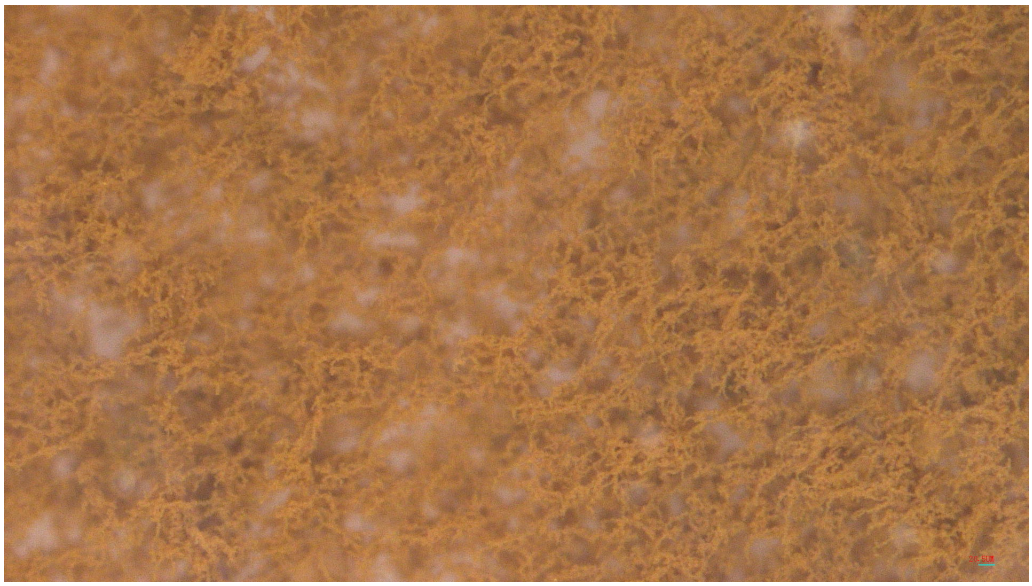

Figure 5.22: CMX-40-10 of Average Diameter 4μm as Captured by Dissection Microscope

Figure 5.23: CMX-10-10 of Average Diameter 1.17μm as Captured by Dissection Microscope

5.3 Building Microcapillary Channels

Two types of microfluidic chip designs have been used to study the different parameters of the beads. In order to build these microfluidic channels, the materials used have been described below.

- PET: Full form of PET is Polyethylene terephthalate. It is a type of high-clarity polyester film "with both of its sides pre-treated to promote adhesion"Tekra (2020).Two types of PET with varying thickness of 3 mil and 7 mil had been used for building the chips. Melinex 454 3 mil (75 micron) PETs were usually used as the top and bottom layers for each of the microfluidic chips. The other one was Melinex 454 7 mil (175 micron) PET which was used in every alternate layer of the chip.

- Adhesives: Three types of adhesives were used in order to bring about variation in the type of microfluidic chips being used.

  - 3M #9965 Microfluidic Diagnostic Tape - This is a double-coated white medical grade PSA purchased from 3M Diagnostic Tapes. The adhesive type is acrylate; total thickness of the purchased material is 3.4 mil and adhesive/PET thickness is 2 mil.

  - AR 90445Q Spacer Tape Adhesive- This is a doubled-coated clear medical grade PSA used to create capillary channels in diagnostic devices in order to maintain accurate sample flow and volume through the channels. This tape was purchased from Adhesives Research.The adhesive type is acrylic.The different layers of the adhesive tape has been shown in figure 5.24. These type of adhesives are popularly used in the assembly of in-vitro diagnostics.

Figure 5.24: Different Layers of AR 90445Q Spacer Tape Adhesive. From Adhesives Research Inc (2020)

Layer	Thickness (mil)	Thickness (μm)	Description
Liner	2.0	51	Clear polyester release liner
Adhesive	1.1	28	AS-110 medical grade adhesive
Carrier	1.0	25	Clear polyester carrier
Adhesive	1.1	28	AS-110 medical grade adhesive
Liner	2	51	Clear polyester release liner
Total Thickness	3.3	81	Excluding Liner

Table 5.2: Table Stating Thickness of Individual Layers for AR 90455Q Adhesive Tape. From Adhesives Research Inc (2020)

  - 200MP Adhesive Tape- The manufacturer of 200MP adhesive tape is 3M Diagnotic Tapes. This adhesive is used for handling difficult environmental conditions like extremely high temperatures or exceptionally high chemical resistance (3M (2020)).

- Cricut Maker and Tools - The Cricut Maker was used to cut these different PSA and PET layers according to the different prototypes designed for testing,

5.3.1 Prototypes of the Microfluidic Channels

- Proto M as shown in figure 5.25 was used for measuring the velocities of the different types of beads. Due to its long straight design, it was easier to study the motion of the magnetic beads as they were pipetted into the microfluidic

Layer	Thickness (mil)	Thickness (mm)	Description (if any)
Liner Caliper	2.0	0.051	Release Liner
Faceside Adhesive	2.9	0.074	Interior of roll, exposed when unwound
Carrier	0.5	0.013	Clear polyester carrier
Backside Adhesive	2.3	0.058	Exterior of roll, exposed when liner removed
Total Thickness	5.7	0.14	Excluding Liner

Table 5.3: Table Stating Thickness of Individual Layers for 200MP Adhesive Tape. From 3M (2020)

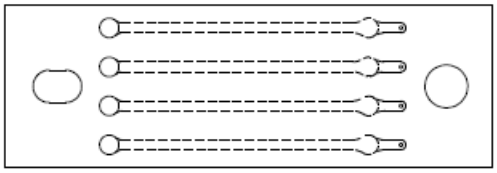

Figure 5.25: Prototype M. Design Courtesy: Clifford Anderson

channels.

- Proto 100040 as shown in figure 5.26 was used for all the other experimental setups- be it the diameter measurements or the one with the syringe pump. The broad analysis well was designed so that a magnet could be placed underneath the channel and the bead movements could be recorded. In the experi-

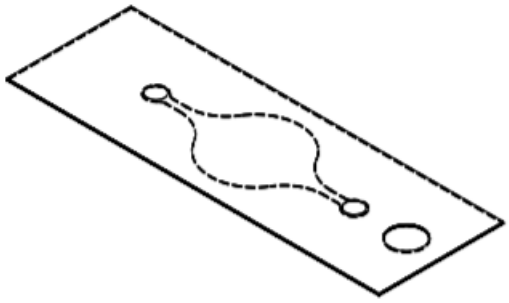

Figure 5.26: Prototype 100040. Design Courtesy: Clifford Anderson

Layer	Type	Material	Thickness (mil)
L01	PET	Melinex 454	3
L02	PSA	3M #9965	3.4
L03	PET	Melinex 454	7
L04	PSA	3M #9965	3.4
L05	PET	Melinex 454	3
		Total Thickness	19.8

Table 5.4: Table Showing Individual Layers for a 5-layered Prototype M Microfluidic Chip

ment where the flow rate of the syringe pump was varied, both 5-layered and 13-layered chips were used for this particular design. For the 13-layered structure, two adhesives- 200MP and AR 90445Q were both tested as it significantly changed the build of the chip. The analyses of those experiments have been described in Chapter 6 in detail. Table 5.6 shows the 13-layered structure of Proto 100040 using 200MP as the adhesive. When AR 90445Q adhesive was used instead of 200MP, thickness of 13-layered chip decreased to 60.2 mil as

carrier thickness for AR 90445Q is 1.0 mil and adhesive thickness is 1.1 mil as shown in table 5.2

Layer	Type	Material	Thickness (mil)
L01	PET	Melinex 454	3
L02	PSA	200MP	5.7
L03	PET	Melinex 454	7
L04	PSA	200MP	5.7
L05	PET	Melinex 454	3
		Total Thickness	24.4

Table 5.5: Table Showing Individual Layers for a 5-layered Prototype 100040 Microfluidic Chip

5.4 Experimental Setup with Varying Flow Rate in Syringe Pump

Materials used for this experimental setup are as follows:-

- Syringe Pump: The model used was KDS 200/200P Legacy Syringe Pump Dual syringe, Infusion Pump from kdScientific Syringe Pumps & Dispensers
- Syringes used were 60ml and 3ml syringes from
- Dispensing needle tips which were used for the syringes
- Grace Bio-Labs press-fit tubing connectors which were fit at the entry and exit points of the channel for smooth flow of the bead solution and water

The setup for this particular experiment has been depicted in figures 5.27 and 5.28.

Layer	Type	Material	Thickness (mil)
L01	PET	Melinex 454	3
L02	PSA	200MP	5.7
L03	PET	Melinex 454	7
L04	PSA	200MP	5.7
L05	PET	Melinex 454	7
L06	PSA	200MP	5.7
L07	PET	Melinex 454	7
L08	PSA	200MP	5.7
L09	PET	Melinex 454	7
L10	PSA	200MP	5.7
L11	PET	Melinex 454	7
L12	PSA	200MP	5.7
L13	PET	Melinex 454	3
		Total Thickness	75.2

Table 5.6: Table Showing Individual Layers for a 13-layered Prototype 100040 Microfluidic Chip Using 200MP as the Adhesive

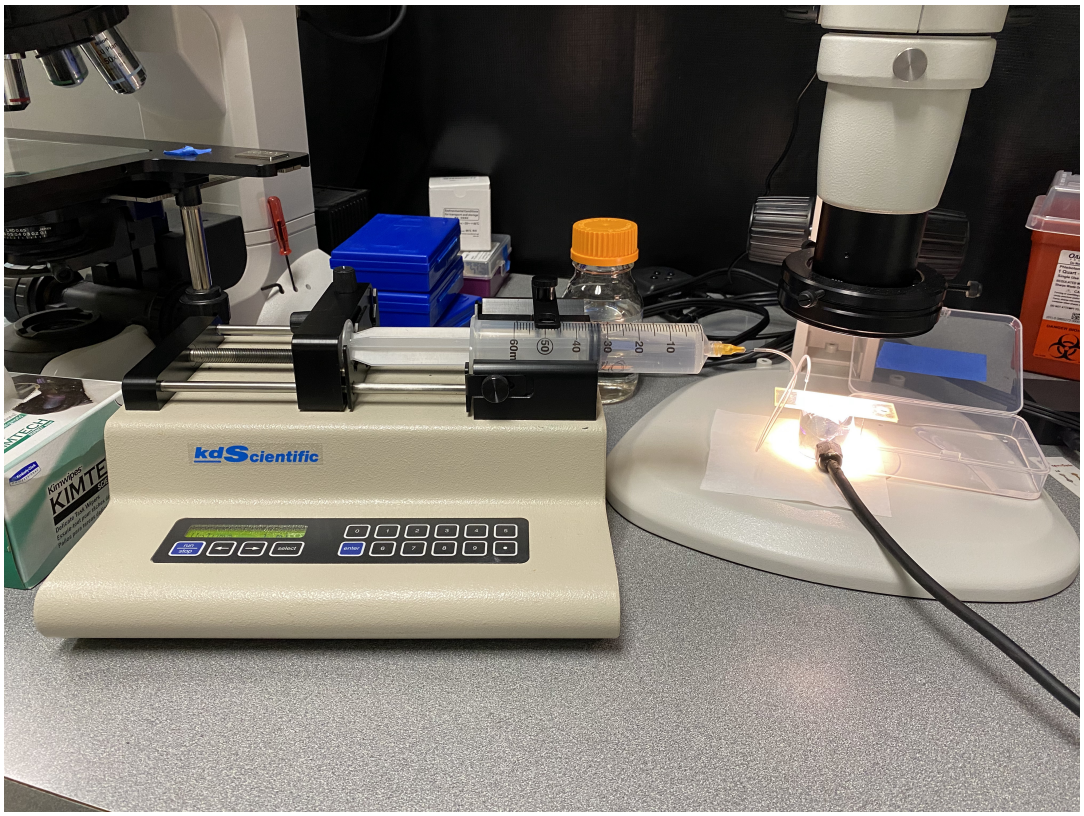

Figure 5.27: Entire Setup of the Experiment with the kdScientific Synringe Pump

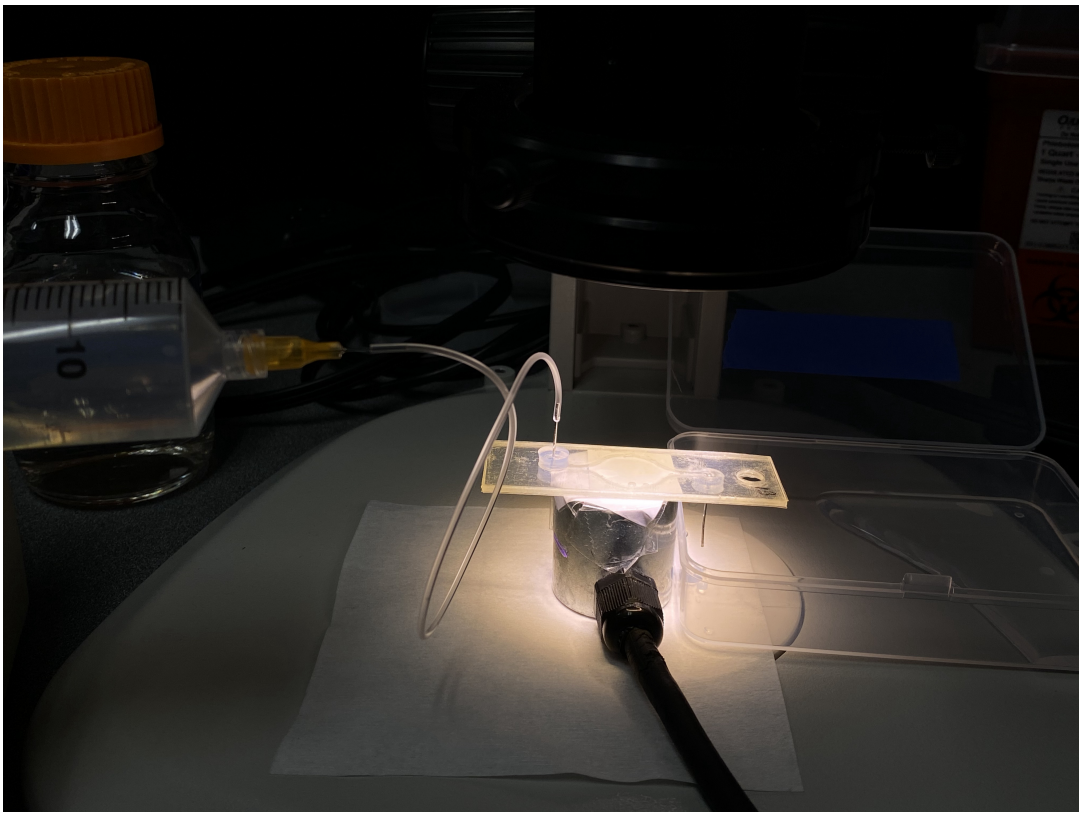

Figure 5.28: Setup with the Microfluidic Chip and Water Being Pushed Through the 60ml Syringe

Chapter 6

RESULTS AND DISCUSSION

6.1 Measuring Different Parameters of the Magnetic Beads

6.1.1 Diameter

The three bigger sized paramagnetic beads from Spherotech Inc. were studied under both the compound and dissecting microscopes mentioned earlier. The diameters of the beads were calibrated under the microscope with respect to a reference measurement. The table 6.1 shows that the average diameter calibrated for CMX-1000-10, CMX-300-10 and CMX-200-10 are more or less around the average diameter specified by Spherotech Inc. in their datasheets. Since CMX-40-10 and CMX-10-10 have average diameters of 4 μm and 1.17 μm respectively according to the datasheet specifications, it was difficult to capture individual beads under the microscope and thus calibrate them. Hence, the diameters of the smaller sized beads could not be verified.

6.1.2 Velocity

The velocities of five different types of beads were measured in three different scenarios which have been shown in the graph 6.1. The Proto M microfluidic chip was used for this experiment to calculate the velocity of the beads using a dissection microscope.

The first scenario was the bead solution being pipetted into the channel and calculating the velocity of the beads based on the distance they covered in a given time period. That has been described by the legend **Without Magnet, Bead**

Type of Bead	Average Diameter Specified by Spherotech Inc. (μm)	Average Diameter Measured (μm)	Standard Deviation
CMX-1000-10	103	99.79	5.68
CMX-300-10	32.2	31.8	1.96
CMX-200-10	18.5	19.43	1.81

Table 6.1: Table Showing the Diameter and the Standard Deviation for Each of the Bigger Sized Magnetic Beads

Solution in 6.1. It says without magnet because no magnet was used to pull the beads from one end of the channel to the other. The motion of the beads without any external force was captured in this part.

In the second scenario, the magnetic beads were diluted in water in 1:2 ratio (400 μm of beads in 800 μm of water). This second scenario has been described as **Without Magnet, Bead diluted in water** in 6.1. It is observed from the plot too that for most of the beads except for the smallest sized one, the velocities calculated in the second scenario are more than that of the first scenario. This is because the velocity of water is adding up to the velocity of the beads which make the movement of the beads through the microfluidic channel easier. As a result of this, the beads start moving faster through the channel as compared to the first setup.

The third and last setup of the scenario had been in presence of a ceramic magnet. A permanent magnet was aligned to one side of the microfluidic channel and the movement of the beads captured with the microscope. It might be believed that the presence of a magnet would have accelerated the motion of the beads to a large extent, but that did not hold true for any of the beads excepting CMX-40-10, according to

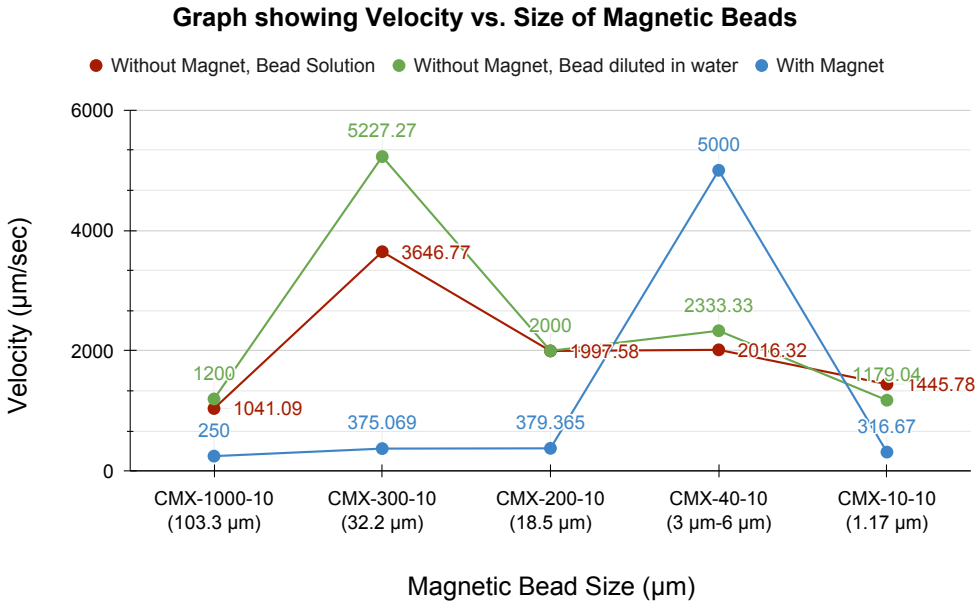

Figure 6.1: Velocity Measurement of the Magnetic Beads in Three Different Scenarios

the plot. This was because the beads showed irregular behaviour in this scenario. Though some of the beads were getting attracted to the magnet almost instantly and moved in less than a second, some of them took quite some time to move. Also, there were collisions between the beads as all of them accumulated at the same spot which was instrumental in causing a hindrance to the smooth motion of the beads. That explains the unexpected behaviour of most of the beads in the plot when an external magnetic force was applied. The legend **With Magnet** represents the values calculated in this scenario. From the graph therefore, we can conclude that, 4 μm beads showed highest velocity in presence of magnet while 32.2 μm beads showed best movement in absence of one.

6.1.3 Calculation of Hydrodynamic Drag Force

The hydrodynamic drag force can be calculated from the velocity values mentioned above using the following equation:-

$$\vec{F}_{hydro} = 6\pi\eta R_{bead}(\vec{v}_{bead} - \vec{v}_{fluid}) \tag{6.1}$$

where $\vec{F}_{hydro}$ is the hydrodynamic force on the beads, R_{bead} is the radius of the bead, η is viscosity of the fluid, $\vec{v}_{bead}$ and $\vec{v}_{fluid}$ are the velocities of the particle and the fluid medium respectively. For our experiments, water is the fluid medium whose η is given as 10e-3 kg.(m.s)$^{-1}$. The hydrodynamic drag force needs to be less than the external magnetic field applied, in order to hold the beads tightly to the magnet which is a necessary feature for the proper extraction of the nucleic acids. Table 6.2 shows the values of the hydrodynamic drag force calculated with respect to each of the different size of carboxyl-coated cross-linked paramagnetic beads. We can observe that with the decreasing size, the hydrodynamic drag force has also decreased.

6.2 Analysis of times of Attraction for Different Beads with Permanent Magnets of Different Magnetic Strengths

The extraction process of nucleic acids consist of multiple washing steps - first with wash solution and then twice with 80% ethanol, which make it absolutely necessary that the beads be tightly held by the permanent magnet(s) as the supernatant is pipetted out of the microcapillary channel or the vial, whichever may be the case. Another important feature for the beads is that they need to get attracted to the permanent magnets quickly. The following two experements with the permanent magnets and the syringe pump flow rates, focus on re-creating the last few steps of the extraction process in order to better understand the magnetic bead characteristics and how they would behave if integrated inside the microcapillary channel of a PoC

Magnetic Bead Type	Hydrodynamic Drag Force (Newton)
CMX-1000-10 (103 μm)	8.31x10e-10
CMX-300-10 (32.2 μm)	6.27x10e-10
CMX-200-10 (18.5 μm)	3.65x10e-10
CMX-40-10 (4 μm)	6.41x10e-11
CMX-10-10 (1.17 μm)	1.89x10e-11

Table 6.2: Table Showing the Hydrodynamic Drag for Calculated Corresponding to Each Bead Type

device.

In each of the bar charts 6.2, 6.3 and 6.4, the x-axis depicts the time taken in seconds by each of the magnetic bead (5 paramagnetic beads from Spherotech and 1 dynabead from Thermo Fisher) to get attracted and agglomerate on one side of the vial when each of the permanent magnet types is used to attract them. The y-axis shows which specific permanent magnet was used. The tables 6.3, 6.4 and 6.5 on the other hand, state the magnetic properties of each of these permanent magnets stated in the bar graphs.

It can be stated thus, the less time a magnetic bead takes to get attracted to the magnet, the better it is in terms of performance. It is observed therefore, that

samarium cobalt being the strongest type of permanent magnets when compared to ceramic and alnico ones, get a consistent response from each of the beads, no matter what size they are. But for the ferrite (ceramic) or alnico magnets nevertheless, the bar graphs show 0 values for some of the beads and permanent magnet combination. This does not mean that it took them milliseconds to get attracted to the magnets. On the contrary, it means that they showed no attraction at all. This means that those permanent magnets did not have enough magnetic field strength to attract that particular bead type. For example, CMX-1000-10, CMX-200-10 and CMX-10-10 were not attracted when alnico magnet 5704K18 and these fields have been marked as NA, which stands for NOT APPLICABLE in table 6.4.

Ceramic Magnet Type	Maximum Pull (lbs)	Maximum Energy Product (kJ/m^3)	Flux Density (Gauss)	**Time taken to agglomerate (secs)**					
				CMX-1000-10	***CMX-300-10***	***CMX-200-10***	***CMX-40-10***	***CMX-10-10***	***Dynabeads***
5857K14	0.5	8.4	2300	NA	NA	NA	26	NA	40
5857K15	4	28	2300	14	18	25	5	52	13
5857K25	0.4	40	3800	30	16	63	10	80	30
5857K26	1	40	3800	19	27	24	4	84	21
5857K28	3	40	3800	20	20	28	2	60	17
5857K21	8	40	3800	18	36	100	8	90	50
5857K22	12	40	3800	22	35	66	6	120	35

Table 6.3: Time Taken by Magnetic Bead Types to Get Attracted to Ceramic Magnets of Varying Magnetic Strengths

Looking closely at the tables and the bar graphs, it can be inferred that when it comes to being attracted to the magnets, CMX-300-10 (32.2 μm sized beads) and CMX-40-10 (4 μm sized beads) show the most consistent behaviour and the best performance. They get attracted to all the magnets within a few seconds, no matter what the magnetic flux density is. CMX-40-10 also does not disperse easily and stay agglomerated for a long time even after the removal of the magnet, clustered together

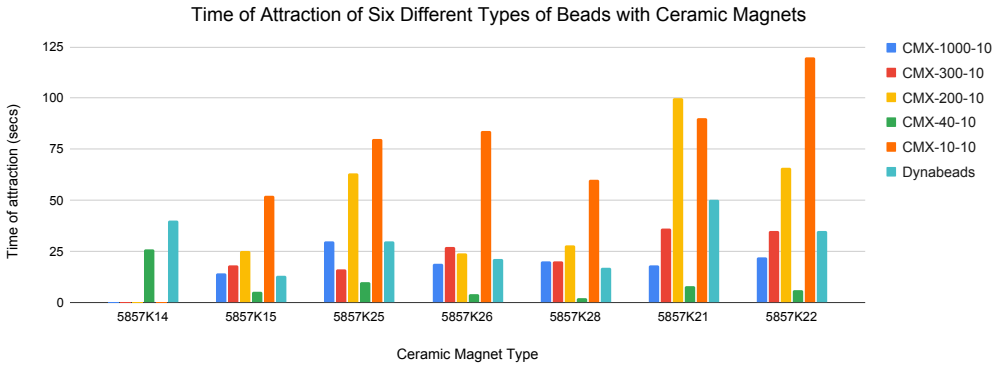

Figure 6.2: Bar Graph Showing the times of Attraction for Six Types of Magnetic Beads with Respect to Ceramic Magnets of Varying Magnetic Strengths

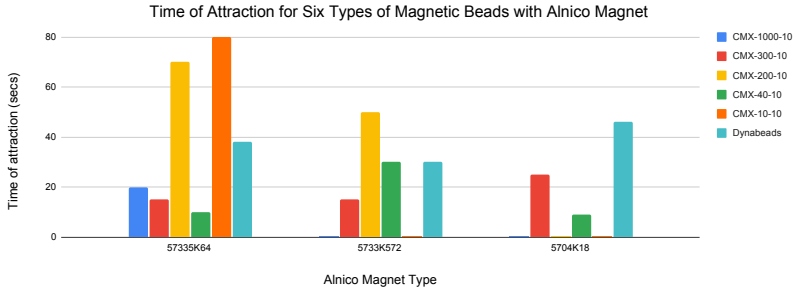

Figure 6.3: Bar Graph Showing the times of Attraction for Six Types of Magnetic Beads with Respect to Alnico Magnets of Varying Magnetic Strengths

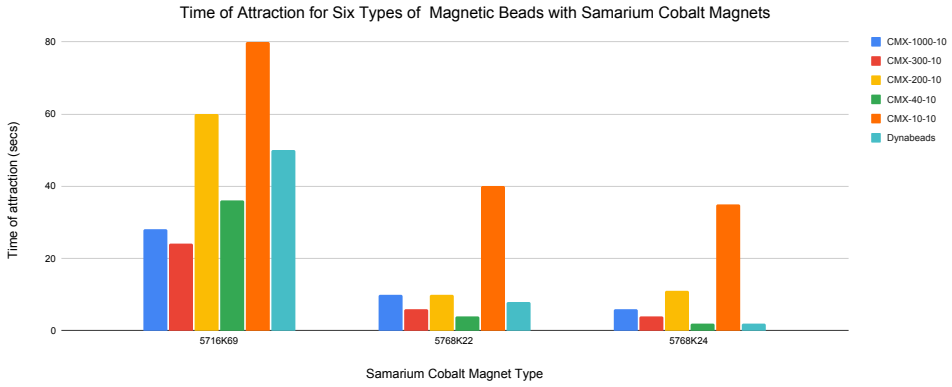

Figure 6.4: Bar Graph Showing the times of Attraction for Six Types of Magnetic Beads with Respect to Samarium Cobalt Magnets of Varying Magnetic Strengths

Alnico Magnet Type	Maximum Pull (lbs)	Maximum Energy Product (kJ/m^3)	Flux Density (Gauss)	**Time taken to agglomerate (secs)**					
				CMX-1000-10	***CMX-300-10***	***CMX-200-10***	***CMX-40-10***	***CMX-10-10***	***Dynabeads***
57335K64	0.1	27	7000	20	15	70	10	80	38
57335K72	0.8	28	7000	NA	15	50	30	NA	30
5704K18	6	46	13000	NA	25	NA	9	NA	46

Table 6.4: Time Taken by Magnetic Bead Types to Get Attracted to Alnico Magnets of Varying Magnetic Strengths

Samarium Cobalt Magnet Type	Maximum Pull (lbs)	Maximum Energy Product (kJ/m^3)	Flux Density (Gauss)	**Time taken to agglomerate (secs)**					
				CMX-1000-10	***CMX-300-10***	***CMX-200-10***	***CMX-40-10***	***CMX-10-10***	***Dynabeads***
5716K69	0.5	143	8600	28	24	60	36	80	50
5768K22	5	199	10,300	10	6	10	4	40	8
5768K24	16	199	10,300	6	4	11	2	35	2

Table 6.5: Time Taken by Magnetic Bead Types to Get Attracted to Samarium Cobalt Magnets of Varying Magnetic Strengths

on one side of the vial, until and unless the vial is shaken rigorously or vortexed.

6.3 Analysis with Varying Syringe Pump Flow Rates

In this section, the behaviour of the magnetic beads with respect to the flow rates of the elution buffer pushed into a microcapillary channel have been analyzed. The five permanent magnet types chosen were based on the last experiment as these are the magnets which attracted the different sized magnetic beads very quickly and were the best among the lot. The first table 6.6 shows the behaviour of the largest sized beads, CMX-1000-10, when put into a 13-layered microfluidic chip built with the 200MP adhesive and pressed moderately. The chip could not bear a flow rate

pressure higher than 40 ml/min and started bending as early as 30 ml/min. The flux density of the electromagnet is unknown. In general terms, lesser the strength of the magnetic field, easier will be to break the clusters of the beads as the pressure of the elution buffer or water in this case needs to overcome the magnetic force applied on the beads to break them apart from the cluster. This means that if the beads break off at a lower flow rate, it means that either the magnet strength is weaker when it comes to attracting a particular type of magentic bead.

Magnet Type	Maximum Pull(lbs)	Flux Density (Gauss)	**Syringe Pump Flow Rates for CMX-1000-10 (ml/min)**		
			Movement of Bead Starts	***Breaking of Cluster Starts***	***Entire Cluster Breaking Point***
Electromagnet	40		11	22.5	25
Ceramic	0.4	3800	0.5	10	25
Ceramic	1	3800	5	12.5	15
Alnico	0.1	7000	5	30	> 30
Samarium-Cobalt	5	10,300	10	40	> 40

Table 6.6: Behaviour of CMX-1000-10 Beads with Varying Flow Rates of Elution Buffer Pushed in a 13-layered Microfluidic Chip Built with Adhesive 200MP

For the next size of beads with an average diameter of 32.2μm and denoted by CMX-300-10, two types of microfluid chips were used; one being a 5-layered one and the other a 13-layered one. The 5-layered microfluidic chip did not work well and broke fairly quick with the increasing flow rate. Comparing tables 6.6 and 6.7, it can be concluded that with increasing flux density, usually the beads are starting to break off from the cluster at a higher flow rate proving the fact that more hydrostatic pressure is being required to overcome the magnetic force attracting the beads into a clustered formation. Also, comparing the two largest sizes of magnetic beads, it is noticed that it is harder to displace CMX-300-10 beads from a clustered formation compared to

CMX-1000-10. This supports the analyses from the previous experiments.

Another noticeable fact for this experiment is that the 13-layered chip used for the CMX-300-10 beads was pressed much more tightly than the previous setup, as a result of which the chip could handle more pressure this time.

Magnet Type	Maximum Pull(lbs)	Flux Density (Gauss)	**Syringe Pump Flow Rates for CMX-300-10 (ml/min)**		
			Movement of Bead Starts	***Breaking of Cluster Starts***	***Entire Cluster Breaking Point***
Electromagnet	40		14	15	25
Ceramic	0.4	3800	15	18	25
Ceramic	1	3800	10	16	20
Alnico	0.1	7000	20	22	25
Samarium-Cobalt	5	10,300	15	22	> 30

Table 6.7: Behaviour of CMX-300-10 Beads with Varying Flow Rates of Elution Buffer Pushed in a 13-layered Microfluidic Chip Built with Adhesive 200MP

For the CMX-200-10 magnetic beads as shown in table 6.8, a new adhesive AR90445Q was used instead of the 200MP one. This chip did not work as well as was expected but it is believed that it was due to the chip not being pressed tightly enough. The layers came off and the chip started warping even at a flow rate of as low as 0.5 ml/min. It is not sure therefore, whether the beads broke off from the cluster due to the warping of the chip or because of the hydro-static pressure from the water being pushed in.

Table 6.9 has been recorded with a 13-layered microfluidic chip with the adhesive AR90445Q and was pressed extremely well, as a result of which it could bear a flow rate as high as 60 ml/min and showed no warping or bending as long as the elution buffer was pushed at a rate lower than 60 ml/min. The magnetic beads CMX-40-10 were fantastic too as they did not break off from the cluster even when

Magnet Type	Maximum Pull(lbs)	Flux Density (Gauss)	**Syringe Pump Flow Rates for CMX-200-10 (ml/min)**		
			Movement of Bead Starts	***Breaking of Cluster Starts***	***Entire Cluster Breaking Point***
Electromagnet	40		10	25	26
Ceramic	0.4	3800	0.5	20	22.5
Ceramic	1	3800	12.5	27.5	30
Alnico	0.1	7000	10	15	30
Samarium-Cobalt	5	10,300	15	30	> 35

Table 6.8: Behaviour of CMX-200-10 Beads with Varying Flow Rates of Elution Buffer Pushed in a 13-layered Microfluidic Chip Built with Adhesive AR90445Q

the chip started bending. This supports the earlier conclusion too from the previous experiment, that these beads got attracted to all the magnets irrespective of their magnetic field strength and flux density and also took the least time to agglomerate on one side of the vial. Even in this experiment, these beads do not show movement or break off from the cluster for most of the magnets.

Magnet Type	Maximum Pull(lbs)	Flux Density (Gauss)	**Syringe Pump Flow Rates for CMX-40-10 (ml/min)**		
			Movement of Bead Starts	***Breaking of Cluster Starts***	***Entire Cluster Breaking Point***
Electromagnet	40		10	15	20
Ceramic	0.4	3800	No Movement	No Movement	> 40
Ceramic	1	3800	15	Cluster did not break	> 60
Alnico	0.1	7000	No Movement	No Movement	> 40
Samarium-Cobalt	5	10,300	No Movement	No Movement	> 40

Table 6.9: Behaviour of CMX-40-10 Beads with Varying Flow Rates of Elution Buffer Pushed in a 13-layered Microfluidic Chip Built with Adhesive AR90445Q

Tables 6.10 and 6.11 depict the setups for CMX-10-10 and dynabeads within a 13-layered microfluidic chip with 200MP being used as the adhesive. Both the chips worked fairly well, though the dynabeads showed better behaviour among the two. Even the chip bending did not break off the dynabeads from the cluster, though the beads did start wiggling a bit.

Magnet Type	Maximum Pull(lbs)	Flux Density (Gauss)	**Syringe Pump Flow Rates for CMX-10-10 (ml/min)**		
			Movement of Bead Starts	***Breaking of Cluster Starts***	***Entire Cluster Breaking Point***
Electromagnet	40		7	10	> 30
Ceramic	0.4	3800	25	29	30
Ceramic	1	3800	20	25	30
Alnico	0.1	7000	35	Cluster did not break	40
Samarium-Cobalt	5	10,300	7	10	> 30

Table 6.10: Behaviour of CMX-10-10 Beads with Varying Flow Rates of Elution Buffer Pushed in a 13-layered Microfluidic Chip Built with Adhesive 200MP

Magnet Type	Maximum Pull(lbs)	Flux Density (Gauss)	**Syringe Pump Flow Rates for Dynabeads (ml/min)**		
			Movement of Bead Starts	***Breaking of Cluster Starts***	***Entire Cluster Breaking Point***
Electromagnet	40		10	25	35
Ceramic	0.4	3800	30	37	> 50
Ceramic	1	3800	No Movement	No Movement	> 40
Alnico	0.1	7000	40	42	45
Samarium-Cobalt	5	10,300	No Movement	No Movement	> 50

Table 6.11: Behaviour of Dynabeads with Varying Flow Rates of Elution Buffer Pushed in a 13-layered Microfluidic Chip Built with Adhesive 200MP

6.4 Extraction of Salmon DNA Using Magnetic Beads

After the characteristic evaluation of beads suitable for PoC device, the nucleic acid extraction of the beads was quantitatively measured using Agilent Tapestation. Sample volumes of 100 μl were extracted and concentrated to 20 μl with different beads. The commercially available dynabeads, which are similar to the paramagnetic beads, are already functionalized specifically for nucleic acid attraction. This results in higher nucleic acid yield in dynabeads compared to other beads. Future studies will be done for extraction efficiency of the beads CMX-300-10 and CMX-40-10 to compare with the commercial beads after functionalization.

Sample	Concentration(pg/μl)
Salmon DNA (Not Concentrated)	1620
CMX-1000-10 (103 μm)	42.5
CMX-300-10 (32.2 μm)	48.2
CMX-200-10 (18.5 μm)	31.6
CMX-40-10 (4 μm)	54.8
CMX-10-10 (1.17 μm)	1090
Dynabeads (1 μm)	6430

Table 6.12: Salmon DNA Extraction

Concluding, it can be said that CMX-40-10 showed the best performance closely followed by the dyanbeads and CMX-300-10. Though the yield efficiency shown in the table **??** proves that the dynabeads and CMX-10-10 have been successful in extracting a better concentration of salmon DNA, but that can primarily be because of the factor that they are smaller in size and hence their concentration had been more when 5 μl of beads were pipetted out. The concentration for the bigger beads need to be calculated accordingly to make them equivalent to the smaller sized beads. We anticipate that we will be able to achieve better or similar yield efficiency as the

dynabeads by varying the concentration of the larger carboxyl-coated paramagnetic beads in future experiments.

Chapter 7

CONCLUSION AND FUTURE WORK

Through this thesis project, it can be concluded that among the paramagnetic beads both the 4 μm CMX-40-10 and 32.2 μm CMX-300-10 are the best, when it comes to being attracted by magnets easily and then being held onto one side for a longer period of time as the external magnetic force is removed, thus allowing for efficient extraction of nucleic acids. The size of the beads do not have any linear relationship however, with that of the varying magnetic field strengths.

Moreover, the larger sized beads including CMX-300-10 has one major disadvantage when it comes to being used for the extraction process. Due to the magnetic beads being larger in size, when 5 μl of bead solution is pipetted into water, the concentration of the larger beads present is much less when compared to an equivalent 5 μl of smaller sized bead solution. The extraction process consists of a lot of steps which requires multiple steps of washing and often, some magnetic beads are lost in this multi-step process. Keeping this in mind, either a higher concentration of larger sized bead solution needs to be used for the extraction process or the risk remains whether enough beads will be left over still, at the end of the entire extraction and isolation process, holding the nucleic acids bound to them.

The dynabeads with their silica coating is the industrial standard used by most people for extracting nucleic acids from bio-samples. It has a very high yield efficiency as has been observed from the results obtained, for the extraction of Salmon DNA mentioned towards the end of the previous chapter. We do believe that we will be able to achieve similar yield efficiency as the dynabeads by varying the concentration of the larger paramagnetic beads.

From the second angle of the thesis project i.e. the electromagnetic point of approach, it can be safely inferred that developing an electromagnetic circuit which would be capable of generating a magnetic field strong enough to attract the beads and also at the same time, be small in size to fit inside a PoC device is quite a bit of a challenge. The literature review in Chapter 4 delves into an area of developing an integrated BioMEMS chip with both electromagnetics and microfluidics embedded in a integrated circuit. Research has been going on in this field for a long time now and embedding electromagnetic features on an integrated circuit using PDMS channels or other methods of fabrication can be an area worth looking into.

It is known that magnetic beads have varied applications in biomedical field starting from magnetic cell separation, extraction and isolation of proteins, targeted drug delivery to brain or malignant tumors, magnetic chaining etc. Even in the extraction and isolation of nucleic acids, the usage of magnetic beads are preferred because it allows for extraction of higher concentration of nucleic acids even from a small amount of bio-sample collected from the human body. In short, the yield is better when magnetic beads are used. This feature, if properly integrated into a point-of-need testing device, would make it much more cost-efficient and robust. Given the current situation of the pandemic, people are in dire need of testing kits, which will allow them to get themselves tested within the comfort of their homes, thus, allowing them to reduce the spread of the disease. The results of this work, therefore, are being used as a guidance to the design of a point of care assay which would be able to detect the presence of viral RNA from the SARS-CoV-2 virus in the human sample collected. In conclusion, I would like to add that, furthering this research will, therefore, increase the sensitivity and specificity of point-of-care devices as a whole.

REFERENCES

Magnetic Microparticles Used in Molecular and Cellular Isolations, Spherotech Inc., URL https://www.spherotech.com/Magnetic\%20Microparticles\%20Used\%20in\%20Molecular\%20and\%20Cellular\%20Isolations.pdf, technical Datasheet (2021a).

Spherotech Paramagnetic Particles, Spherotech Inc., URL https://spherotech.com/2020\%20Product\%20Detail\%20Pages/Spherotech\%20Paramagnetic\%20Particles.pdf, technical Datasheet (2021b).

3M, E. o. M., "3m-double-coated-tape-9495mp", URL https://www.3m.com/3M/en_US/company-us/all-3m-products/~/3M-Double-Coated-Tape-9495MP/?N=5002385+3290918216&rt=rud (2020).

Adhesives Research Inc, E. o. A. R. I., "Arcare®-90445q-product-information-sheet", URL https://www.adhesivesresearch.com/wp-content/uploads/2020/11/ARcare\%C2\%AE-90445Q-Product-Information-Sheet.pdf (2020).

antibodies online.com, E. o. a.-o., "Magnetic beads", URL https://www.antibodies-online.com/resources/17/5035/magnetic-beads/ (2021).

Biosan, E. o. B., "Biomagpure 12 plus", URL https://biosan.lv/products/biomagpure-12-Plus/ (2021).

Britannica, T. E. o. E., "Polymerase chain reaction", URL https://www.britannica.com/science/polymerase-chain-reaction\#/media/1/468736/18071 (2019).

Byrnes, S. A., J. D. Bishop, L. Lafleur, J. R. Buser, B. Lutz and P. Yager, "One-step purification and concentration of dna in porous membranes for point-of-care applications", Lab on a Chip **15**, 12, 2647–2659, URL https://doi.org/10.1039/C5LC00317B (2015).

ElectronicsTutorials, E. o. E., "Electromagnetism", URL https://www.electronics-tutorials.ws/electromagnetism/magnetism.html (2013).

Herbst, J. F., "Permanent magnets", American Scientist **81**, 3, 252–260, URL http://www.jstor.org.ezproxy1.lib.asu.edu/stable/29774920, full publication date: May-June 1993 (1993).

Microscope World, E. o. M. W., "What is a compound microscope", URL https://www.microscopeworld.com/p-3470-what-is-a-compound-microscope.aspx (2021).

Microscope.com, E. o. M., "Dissecting microscopes", URL https://www.microscope.com/specialty-microscopes/dissecting-microscopes (2021).

Ruffert, C., "Magnetic bead—magic bullet", Micromachines **7**, 2, URL https://www.mdpi.com/2072-666X/7/2/21 (2016).

Siegel, A. C., S. S. Shevkoplyas, D. B. Weibel, D. A. Bruzewicz, A. W. Martinez and G. M. Whitesides, "Cofabrication of electromagnets and microfluidic systems in poly(dimethylsiloxane)", Angewandte Chemie International Edition **45**, 41, 6877–6882, URL https://onlinelibrary.wiley.com/doi/abs/10.1002/anie.200602273 (2006).

Tekra, E. o. T., "melinex-454", URL https://www.tekra.com/products/films/polyester-films/polyester-pet/melinex-454 (2020).

Wikipedia contributors, "Beat frequency oscillator — Wikipedia, the free encyclopedia", URL https://en.wikipedia.org/w/index.php?title=Beat_frequency_oscillator&oldid=1014708420, [Online; accessed 28-March-2021] (2021a).

Wikipedia contributors, "Phase-contrast microscopy — Wikipedia, the free encyclopedia", https://en.wikipedia.org/w/index.php?title=Phase-contrast_microscopy&oldid=1006157914, [Online; accessed 1-April-2021] (2021b).

Wikipedia contributors, "Spin column-based nucleic acid purification — Wikipedia, the free encyclopedia", https://en.wikipedia.org/w/index.php?title=Spin_column-based_nucleic_acid_purification&oldid=1007169448, [Online; accessed 6-April-2021] (2021c).

Zheng, Y., A. Mannai and M. Sawan, "A biomems chip with integrated micro electromagnet array towards bio-particles manipulation", Microelectronic Engineering **128**, 1–6, URL https://www.sciencedirect.com/science/article/pii/S0167931714002585 (2014).